NISTIR 89-4161

Applied and
Computational
Mathematics
Division

Center for Computing and Applied Mathematics

Directional Solidification of a Planar Interface in the Presence of a Time-Dependent Electric Current

L.N. Brush, S.R. Coriell and G.B. McFadden

September 1989

U.S. DEPARTMENT OF COMMERCE
National Institute of Standards and Technology
Gaithersburg, MD 20899

Directional Solidification of a Planar Interface in the Presence of a Time-Dependent Electric Current

L. N. Brush, S. R. Coriell and G. B. McFadden

National Institute of Standards and Technology

Gaithersburg, MD 20899, USA

September 20, 1989

Abstract

We develop a numerical method to study the motion of a planar crystal-melt interface during the directional solidification of a binary alloy in the presence of a time-dependent electric current. The model includes the Thomson effect, the Peltier effect, Joule heating and electromigration of solute in the coupled set of equations governing heat flow in the crystal and melt, and solute diffusion in the melt. For a variety of time-dependent currents, the temperature fields and the interface velocity are calculated as functions of time for indium antimonide and bismuth, and for the binary alloys, germanium-gallium and tin-bismuth. For the alloys, we also calculate the solid composition as a function of position, and thus make quantitative predictions of the effect of an electrical pulse on the solute distribution in the solidified material. In addition, for a sinusoidal current of small amplitude, we have compared the numerical solutions with approximate analytical solutions valid to first order in the current amplitude. By using this numerical approach the specific mechanisms which play dominant roles in interface demarcation by current pulsing can be identified.

1. Introduction

A number of effects occur when an electric current is passed through a solidifying sample. In the bulk of the sample, there is Joule heating and, in the presence of a temperature gradient, there is Thomson heating or cooling. In addition, at the crystal-melt interface there is liberation or absorption of heat due to the Peltier effect. The Thomson and Peltier effects are proportional to the current and thus depend on its sign, while Joule heating is proportional to the square of the current. In alloys, electric currents also cause electromigration which modifies the solute distribution. Thus, the passage of an electric current through the sample during crystal growth alters the compositional and thermal profiles in the crystal and in the melt, and also modifies the interface velocity, thereby changing the final properties of the solidified sample. We numerically model the effect of a time-dependent electric current on the directional solidification of a binary alloy with a planar crystal-melt interface. The calculations elucidate the relative importance of various electrical phenomena on the solidification process, namely, the roles of the Thomson effect, the Peltier effect, Joule heating and electromigration of solute.

There have been a number of studies of the effect of an electric current on solidification and crystal growth. Early work on the effects of an electric current on solidification has been described by Pfann[1]. The Peltier effect between crystal and melt was measured in bismuth, cadmium and zinc by passage of a direct current by Bardeen and Chandrasekhar[2]. The effect of a direct current on solute redistribution in bismuth-tin alloys and on interfacial instability in tin-bismuth alloys has been studied by Verhoeven[3, 4]. More recently, electric

currents have been used for the growth of epitaxial layers of gallium-arsenide (liquid phase electroepitaxy, see, for example, reference[5]). The effect of an electrical current on morphological stability has been the subject of a number of recent theoretical investigations[6, 7, 8, 9].

Singh et al.[10] employed current pulsing to mark the crystal-melt interface in tellurium-doped indium antimonide and thus to measure crystal growth rates. This technique has been used to study interface instability in gallium-doped germanium[11] and to measure the Peltier coefficient for indium antimonide[12]. Peltier heating due to a current pulse in a pure material has been numerically modelled by Wargo and Witt[13]; this model has recently been extended by Duffar et al.[14] Thermal measurements in pure bismuth and bismuth-manganese eutectics during electrical pulsing have been carried out by Silberstein et al.[15, 16].

The equations governing alloy solidification are inherently nonlinear since the crystal-melt interface is a free boundary (see, for example, Derby and Brown[17] and references therein). We numerically treat the effect of a time dependent electric current on the planar directional solidification of a binary alloy by performing a transformation of variables which fixes the solid and liquid regions in the transformed domain. The spatial derivatives of the transformed differential equations are replaced with second order accurate finite differences, and the resulting set of equations are then integrated in time using ordinary differential equation integration software. For a variety of time-dependent currents, the temperature fields and the interface velocity as functions of time are presented for indium antimonide and bismuth, and for the binary alloys, germanium-gallium and tin-bismuth. For the alloys,

we also calculate the solid composition as a function of position, and thus make quantitative prediction of the effect of an electrical pulse on the solute distribution in the solidified material. The model also allows us to investigate the role of individual thermoelectric effects; results are presented for bismuth.

2. The Model

We consider the one-dimensional case of the free boundary problem described by Coriell et al.[9], in which the electric current density $I(t')$ is allowed to vary with time, t', and the crystal-melt interface moves along the z' axis. The governing set of differential equations for the temperature $T(z',t')$ and for the composition $C(z',t')$ in the bulk liquid phase are

$$c_{pL}\frac{\partial T_L}{\partial t'} = \lambda_L\frac{\partial^2 T_L}{\partial z'^2} + \frac{I^2}{\sigma_L} - \tau_L I\frac{\partial T_L}{\partial z'}, \tag{1}$$

$$\frac{\partial C_L}{\partial t'} = D_L\frac{\partial^2 C_L}{\partial z'^2} - u\frac{I}{\sigma_L}\frac{\partial C_L}{\partial z'}, \tag{2}$$

while in the solid phase

$$c_{pS}\frac{\partial T_S}{\partial t'} = \lambda_S\frac{\partial^2 T_S}{\partial z'^2} + \frac{I^2}{\sigma_S} - \tau_S I\frac{\partial T_S}{\partial z'} \tag{3}$$

governs heat flow. Diffusion of solute in the solid phase, the density change upon solidification and fluid flow will be neglected. In Eqns. (1) to (3), c_p is the specific heat per unit volume, λ is the thermal conductivity, σ is the electrical conductivity, τ is the Thomson coefficient and u is the differential mobility of solute, with subscripts S and L denoting solid and liquid, respectively.

The compositional and the thermal fields are coupled at the crystal-melt interface $z' =$

$h(t')$, through the boundary conditions

$$T_S - T_L = 0, \tag{4}$$

$$T_L = T_M + mC_L, \tag{5}$$

$$\lambda_S \left(\frac{\partial T_S}{\partial z'}\right) - \lambda_L \left(\frac{\partial T_L}{\partial z'}\right) = L_v \frac{dh}{dt'} + \Pi_{SL} I, \text{ and} \tag{6}$$

$$D_L \left(\frac{\partial C_L}{\partial z'}\right) = \frac{uC_L}{\sigma_L} I - \frac{dh}{dt'}(1-k)C_L, \tag{7}$$

in which $k = C_S/C_L$ is the solute distribution coefficient, T_M is the melting point of the pure material, m is the slope of the liquidus, Π_{SL} is the Peltier coefficient, and L_v is the latent heat of fusion per unit volume. All of the thermophysical properties in eq. (1) through eq. (7) are assumed constant.

During the solidification of a binary alloy, the interfacial temperature is a priori unknown, and must be determined self-consistently from the phase diagram as given by eq. (5). We note that to accurately model the effects of electrical currents sufficiently large to cause melting of an alloy, diffusion in the crystal must be considered. Numerical solution to the set of equations (1) to (7), together with appropriate far-field boundary conditions (discussed below), will determine the position of the crystal-melt interface as a function of time, and will provide the fully time-dependent behavior of the thermal and compositional profiles throughout the sample.

3. Numerical Method

3.1. Variable Transformations

Our numerical solution procedure is implemented by transforming the set of equations (1) to (7) to a moving coordinate system traveling with the sample at velocity V, such that $z = z' - Vt'$ and $t = t'$. In the moving coordinate system the interface position $w(t)$ is given by $w(t) = h(t') - Vt'$. The extent of both the liquid and solid regions is truncated by introducing finite cut-off lengths, where far-field boundary conditions are applied. We have chosen the origin of our coordinate system such that the solid phase lies within the region $0 \leq z \leq w(t)$. We define a thermal cut-off length $z = L_T$ and a solutal cut-off length $z = L_C$. Since the thermal and solutal fields are only coupled at the crystal-melt interface, it is not necessary to take $L_T = L_C$; in order to accurately resolve the solute field and save computational time, L_C will be chosen smaller than L_T. We fix the position of the interface by mapping the crystal and the melt into unit intervals using the transformations $\xi_S = z/w(t)$ in the solid, $\xi_L = [z - w(t)]/[L_T - w(t)] + 1$ in the liquid for the thermal field and $\xi_C = [z - w(t)]/[L_C - w(t)] + 1$ in the liquid for the compositional field.

The equations governing heat flow and diffusion in the melt become,

$$\frac{\partial T_L}{\partial t} = \frac{\lambda_L}{c_{pL}(L_T - w)^2}\left(\frac{\partial^2 T_L}{\partial \xi_L^2}\right) + \frac{V - w_t(\xi_L - 2) - \tau_L I/c_{pL}}{(L_T - w)}\left(\frac{\partial T_L}{\partial \xi_L}\right) + \frac{I^2}{\sigma_L c_{pL}}, \tag{8}$$

$$\frac{\partial C_L}{\partial t} = \frac{D_L}{(L_C - w)^2}\left(\frac{\partial^2 C_L}{\partial \xi_C^2}\right) + \frac{V - w_t(\xi_C - 2) - uI/\sigma_L}{(L_C - w)}\left(\frac{\partial C_L}{\partial \xi_C}\right), \tag{9}$$

respectively, and in the solid the equation governing heat flow becomes

$$\frac{\partial T_S}{\partial t} = \frac{\lambda_S}{c_{pS} w^2}\left(\frac{\partial^2 T_S}{\partial \xi_S^2}\right) + \frac{V + w_t \xi_S - \tau_S I/c_{pS}}{w}\left(\frac{\partial T_S}{\partial \xi_S}\right) + \frac{I^2}{\sigma_S c_{pS}}. \tag{10}$$

with $w_t = dw/dt$. At the crystal-melt interface ($\xi_S = \xi_L = \xi_C = 1$), eqs. (4) and (5) remain unchanged, and eqs. (6) and (7) become:

$$\frac{\lambda_S}{L_v w}\left(\frac{\partial T_S}{\partial \xi_S}\right) - \frac{\lambda_L}{L_v(L_T - w)}\left(\frac{\partial T_L}{\partial \xi_L}\right) = w_t + V + \frac{\Pi_{SL} I}{L_v}, \text{ and} \tag{11}$$

$$\frac{D_L}{(L_C - w)}\left(\frac{\partial C_L}{\partial \xi_C}\right) = \frac{u C_L}{\sigma_L} I - (V + w_t)(1 - k) C_L. \tag{12}$$

Finally, the following mixed boundary conditions are applied at the far-field cutoff lengths

$$\frac{A_L^\infty}{(L_T - w)}\left(\frac{\partial T_L}{\partial \xi_L}\right) + B_L^\infty T_L = E_L^\infty \text{ at } \xi_L = 2, \tag{13}$$

$$\frac{A_C^\infty}{(L_C - w)}\left(\frac{\partial C_L}{\partial \xi_C}\right) + B_C^\infty C_L = E_C^\infty \text{ at } \xi_C = 2, \text{ and} \tag{14}$$

$$\frac{A_S^\infty}{w}\left(\frac{\partial T_S}{\partial \xi_S}\right) + B_S^\infty T_S = E_S^\infty \text{ at } \xi_S = 0. \tag{15}$$

where the quantities with superscript '∞' are constants.

3.2. Discretization

We reduce the coupled set of partial differential equations and interfacial conditions to a system of ordinary differential equations in time by discretizing the spatial derivatives. The spatial derivatives in each of the differential equations (8) to (10) are replaced by second order accurate centered finite differences at equally spaced interior nodes. At the exterior boundaries we apply one-sided second order accurate finite differences as approximations to the first order derivatives in eqs. (13) to (15), and eliminate the temperature and the composition as unknown variables at the sample endpoints.

The conservation of solute boundary condition, eq. (12), is treated by introducing a fictitious nodal point in the solid phase and then using a centered difference approximation

for the derivative of melt composition at the interface. The fictitious nodal point introduces an extra unknown into the problem, and the interfacial composition can be determined by applying the diffusion equation for the bulk liquid phase at the interface as well. Finally, the heat flux condition eq. (11) provides an ordinary differential equation for the interface position; second order accurate one-sided differences are used to evaluate the temperature gradients in the liquid and solid at the interface.

Thus, specifying appropriate experimental and material parameters, including the coefficients in the far-field conditions (Eqns. (13), (14) and (15)), initial data for the temperature and solutal fields and the interface position, we then integrate the ordinary differential equations in time using the software package SDRIV3[18]. This determines the thermal and the solutal fields and the position of the crystal-melt interface as functions of time.

3.3. Absorbing Far-Field Boundary Conditions

In order to accurately resolve the solutal field in front of an advancing interface, we impose a cutoff boundary that is often far shorter than a typical experimental sample length, and is only a few solute decay lengths from the interface. We use the following far-field boundary condition:

$$\frac{D}{(V - [uI/\sigma_L])} \left(\frac{\partial C_L}{\partial z} \right) + C_L = C_\infty, \tag{16}$$

where C_∞ is the concentration of solute in the liquid far from the interface. Eq. (16) is automatically satisfied under steady-state growth conditions in the sample at any value of z. Similar boundary conditions could also be imposed on the thermal fields at the sample

endpoints; however for the calculations reported here we simply fix the temperatures at the outer boundaries using values consistent with steady-state motion.

3.4. Numerical Comparisons to Known Solutions

We compare our numerical results with an analytical solution given by Smith et al.[19] and by Tiller and Sekerka[20] for the initial transient in an initially homogeneous sample solidifying at constant velocity with constant interface temperature (that is, $m = 0$). In our numerical calculations the imposed thermal fields keep the interface moving at constant velocity, and we calculate the solutal profile as it changes from its initially homogeneous state. As in all of our calculations, we use the mixed condition given by eq. (16) at the sample endpoint L_C. We compare our numerical calculations of the interfacial melt composition to eq. (26) of Smith et al.[19] at various times in Table (1) for different values of the mesh spacing. The numerical and the analytical results are in good agreement, and indicate that the numerical method is spatially second order accurate.

We also compare our numerical results to eq. (43a) of Smith et al[19] which represents the changes that the solutal field undergoes when there is an instantaneous change in the interfacial velocity from, say, V_1 to V_2. The initial solute distribution corresponds to the steady-state distribution for velocity V_1. (The liquidus slope m is still assumed to be zero.) We calculate the resulting transient in the solutal field that occurs as the solutal profile adjusts itself to the discontinuous change in the growth speed. Comparison between the analytically and numerically calculated interface compositions as a function of time is given in Table (2) for $L_C = 4D/V_1 = 0.4$ cm. Again, the numerical and the analytical results are in

good agreement, and indicate that the numerical method is spatially second order accurate. The accuracy of our numerical technique for a discontinuous change in the interface velocity indicates that we can accurately calculate the solute profiles under conditions of square wave current pulsing, for which discontinuous changes in the growth velocity also occur.

In the Appendix we derive a linear theory for the case of a small amplitude sinusoidal current of the form $I = I_o + I_1 e^{i\omega t}$, in which ω is the frequency of the oscillation. The solutions are assumed to be of the form,

$$\begin{pmatrix} T_S(z,t) \\ T_L(z,t) \\ C(z,t) \\ w(t) \end{pmatrix} = \begin{pmatrix} T_S^{(0)}(z) \\ T_L^{(0)}(z) \\ C^{(0)}(z) \\ H \end{pmatrix} + \begin{pmatrix} T_S^{(1)}(z) \\ T_L^{(1)}(z) \\ C^{(1)}(z) \\ \delta \end{pmatrix} e^{i\omega t}. \tag{17}$$

The unperturbed solutions (denoted by the superscript '(0)') satisfy the steady-state equations for a constant current I_o and velocity V. For convenience in this calculation we take z = 0 to be the position of the unperturbed interface; the quantity δ measures the deviation of the interface position due to the oscillating current. Eqn. (17) is substituted into the governing equations and boundary conditions given by Eqns. (1) through (7) and the far-field conditions, Eqns. (13) through (15). We expand all the boundary conditions in a Taylor's series about the unperturbed interfacial position retaining only terms that are linear in the coefficients of $e^{i\omega t}$. The resulting linearized set of equations is then solved. A comparison between analytically and numerically calculated growth velocities are given in Table (3), showing agreement between the two calculations.

4. Numerical Results

We carry out numerical calculations for the pure materials indium antimonide, InSb, and bismuth, Bi, and for the binary alloys, germanium-gallium, Ge-Ga, and tin-bismuth, Sn-Bi. The material properties used in our calculations are given in Table (4). For all our calculations, the initial thermal and solutal profiles are the steady-state profiles given by eqs. (21) - (23) in the Appendix.

Numerical calculations for InSb have been carried out by Wargo and Witt[13] and Duffar et al.[14] The thermal fields associated with current pulsing in pure Bi have been studied by Silberstein and Larson[16]. The alloy Ge-Ga has been successfully used by Holmes and Gatos[11] for interface demarcation by current pulsing. Finally, the alloy Sn-Bi has been chosen for experiments in microgravity with the MEPHISTO apparatus[21], which uses current pulsing for interface demarcation.

4.1. Indium Antimonide

The plots in Fig. (1) give the interfacial growth speed $v = dh/dt$ as a function of time. In the top plot in Fig. (1), the initial growth rate is 11.33μm/s and the initial temperature gradient in the melt at the interface is 25.0 K/cm. A current pulse of 20.3 A/cm^2 and of one second duration is applied at 3.0 and 7.0 seconds. In our model, since there is an instantaneous jump in the current (ΔI), there is an instantaneous jump in the microscopic growth rate by an amount $\Delta v = -\Pi_{SL}\Delta I/L_v = 14.6\mu$m/s, since the thermal fields cannot change instantaneously. This discontinuity in the velocity is captured by the numerical

method. As the thermal field relaxes, the velocity decreases by 0.45μm/s, and then a jump in the velocity of the same magnitude but of opposite sign occurs when the current pulse is turned off. In the bottom plot in Fig. (1) we show the results for repeated current pulses of 9.5 A/cm^2 which are on for 20 s and off for 40 s, for which the initial growth rate is 12.0μm/s and the initial temperature gradient in the melt at the interface is 25.0 K/cm. Both calculations shown in Fig. (1) are in close agreement with Wargo's numerical and experimental results. Furthermore, as calculated by Wargo for repeated pulses, the maxima and minima of the velocity of the interface decrease from their initial values as the transients decay; the average growth rate is eventually determined by the overall pulling rate.

4.2. Bismuth

We next investigate the effect of an electric pulse on the interfacial velocity and the thermal fields in the liquid. Furthermore, we isolate the contribution of the Peltier, Thomson and Joule effects by setting the appropriate thermoelectric coefficients to zero. The interface is initially static and the temperatures at the finite cut-off lengths are held fixed. The temperature gradient in the liquid at the interface is initially 100 K/cm and the length L_T is 4 cm with the interface located 1.5 cm from the solid end of the sample. At t = 20 s, a current pulse of + 80 A/cm^2 is applied to the sample for a 10 second duration, as used in the experiments of Silberstein and Larson[16]. The interfacial velocity and the change in temperature at three fixed positions in the liquid, 0.05, 1.25 and 2.27 cm from the initial interface position, are plotted as functions of time in Fig. (2).

Fig. (2) shows that the temperature change near the interface is very different from that

away from the interface, which is in qualitative agreement with experiment[16]. Quantitative comparison between the numerical and experimental results is not possible because of uncertainty in the physical parameters and boundary conditions at the sample endpoints. Figs. (3) and (4) show the individual contributions of the Peltier, Thomson and Joule effects to the temperature change and the interface velocity, respectively. For example, in the top plot for the Peltier effect in Figs. (3) and (4), the Thomson coefficients in the liquid and the solid are zero, and the electrical conductivities in the solid and liquid are infinite. As would be expected from the sign of the Peltier coefficient, a positive current causes cooling in the liquid and an increase in the interface velocity. For bismuth, the Thomson coefficient in the solid is positive, while the Thomson coefficient in the liquid is almost zero but slightly negative (estimated from Fig. (6) of Ubbelohde[22]). Thus the Thomson effect in the solid causes cooling of the sample, and the Thomson effect in the liquid causes heating. From the magnitude of the coefficients, the cooling in the solid dominates, and the interface velocity is increased. Thus the interface moves closer to the point at which the temperatures are measured and the temperatures are lowered even though there is a slight Thomson heating in the liquid. Additional calculations with different values for the Thomson coefficients have verified this interpretation. The Joule heating, which is independent of the sign of the current, causes a temperature rise and a decrease in the interface velocity. While this is a nonlinear problem and the individual contributions are not additive, comparison of Figs. (2) and (4) indicate that immediately following the application of the current, the Peltier effect dominates, but as the temperature field relaxes, the Thomson effect and the opposing Joule

effect provide relatively constant contributions to the interface velocity as well. Fig. (3) shows that away from the interface Joule heating is dominant, but the heating is suppressed near the sample end (upper curve in each plot), due to the constant temperature boundary condition. In Fig. (2), the change in temperature decays to zero after the current pulse is turned off. This behavior depends on the boundary conditions at the sample endpoint; if, for example, we had used no flux conditions, there would have been a net change in the temperature of the sample.

Figs. (5) - (7) are analogous to Figs. (2) - (4) except that the current is of opposite sign. In this case, all effects act to increase the temperature in the liquid as shown in Fig. (6), with the largest temperature change occurring near the crystal-melt interface. At the beginning of the current pulse, the interface velocity is negative, decreases in magnitude, but remains negative due to the heating until the current pulse ends.

In Figs. (2) and (5), the temperature change near the interface is neither symmetric nor anti-symmetric with respect to a change in sign of the current pulse. If Joule heating were dominant, symmetric behavior would be expected, while if Joule heating were unimportant, anti-symmetric behavior would be expected.

4.3. Germanium-Gallium

For the case of alloy solidification, a current pulse modifies the compositional profile in the liquid as well as the interface velocity and the thermal fields in the solid and liquid. The composition in the solid depends on the composition in the liquid at the interface, and is therefore modified by the current pulse. This change in solid composition is the basis of the

interface demarcation technique[10].

We present calculations for Ge-Ga alloys, under different processing conditions. First, we consider the case in which the current is turned on and left on. There is a transient stage in which the system changes from its steady state in the absence of a current to a new steady state for a finite current (see eqs. (21) to (23) of Appendix). The initial and final interface velocities are identical, but the initial and final concentration and temperature fields differ.

In Figs. (8) and (9) a current of ± 25 A/cm^2 is applied at $t = 10$s. The bulk alloy composition is 0.1 at% gallium, the initial temperature gradient in the liquid at the interface is 130 K/cm and the initial interface velocity is 38μ m/s. The temperature changes are measured at three fixed positions (z = constant) in the liquid, 0.02 (lower curves), 0.5 (middle curves) and 0.91 cm (upper curves) from the initial interface position in a moving reference frame, i.e., if the interface continued to move at constant velocity, the points would remain at fixed distances from the interface. For a positive current the Peltier effect provides cooling while the Thompson and Joule effects provide heating. For this alloy, the Peltier effect is dominant and the interface velocity increases upon application of the current which results in an increase in the composition of the solid. Upon the application of a negative current (Fig. (9)), the interface velocity and the composition of the solid initially decrease.

In Figs (10) and (11) we show the effect of different sample compositions on the change in the temperature in the liquid, for the same conditions as for Figs. (8) and (9), respectively. In each figure, the upper plot is for pure germanium, and the middle and lower plots are for germanium containing 0.3 at% and 0.5 at% gallium, respectively. As the composition is

increased the temperature change in the liquid near the interface becomes larger, reflecting the change in interface temperature with solute concentration. The maximum change in temperature is attained more quickly for larger compositions. After the new steady state is attained, the temperature changes are different for positive and negative currents. For a positive current, the interface attains a new position which is closer to the points at which the temperature change is calculated. This, together with the readjustment of the temperature profile due to the electric current, gives rise to the difference in the temperature changes for positive and negative currents.

In the next series of calculations, we study the effect of a current pulse in germanium-gallium with parameters typical of those used for interface demarcation[11], namely, $\pm$ 80 A/cm^2 and 0.1 s in duration. The initial interface velocity is 38 μm/s and the initial temperature gradient in the liquid at the interface is 130 K/cm. Figs. (12) and (13) show the changes in temperature and the interface velocity as functions of time, and the solid composition as a function of distance for positive and negative currents, respectively. For a positive current the Thomson and Joule effects provide heating while the Peltier effect cools the sample. From Fig. (12), it is clear that the Peltier effect dominates near the interface, while away from the interface there is a slight heating. Comparing Figs. (12) and (13), the temperature change near the interface and the interface velocity are almost antisymmetric with respect to a change in the sign of the current, which is consistent with the dominance of the Peltier effect. The interface velocity instantaneously increases (decreases) upon application of a positive (negative) current; it then decreases (increases) rapidly followed by a slow

decay (rise) until the current pulse is over. The composition changes monotonically upon the application of the current and then abruptly begins to return to its initial composition once the current is over. The solute composition in the solid has a maximum change of about five percent of the bulk solute concentration. The solid composition changes over a distance of about 10 μm; there are particularly sharp concentration gradients associated with the beginning and end of the current pulse.

4.4. Tin-Bismuth

In Figs. (14) and (15) a current of $\pm 50 A/cm^2$ is applied for 5 seconds. The bulk alloy composition is 0.78 at%, with an initial temperature gradient in the liquid at the interface of $135 K/cm$ and an initial interface velocity of $1.67 \mu m/s$. The temperature changes are measured at three fixed positions in the liquid, 0.03 (lower curves), 0.75 (middle curves) and $1.36 cm$ (upper curves) from the initial interface position in a moving reference frame. For a positive current the Peltier effect provides cooling; the Thomson effect is essentially negligible for tin. Figs. (14) and (15) show changes in the liquid temperature and the velocity as functions of time, and the composition in the solid as a function of position. The similarity in the thermal profiles for both positive and negative currents indicate that Joule heating is playing the important role in altering growth conditions. For the positive current pulse, after the initial increase due to the Peltier effect, the interfacial velocity sharply decreases to less than its initial value, which is consistent with the important role of Joule heating. Additional calculations with $\Pi_{SL} = 0$ show that the change in temperature and the solid composition are very similar to those shown in Fig. (14). For negative current pulses,

the velocity decreases and remains relatively constant until the pulse is terminated. The composition in the solid is changed by about 2 percent of the bulk value for the negative pulse and somewhat less for the positive pulse, over a distance of about 20 μm.

In the calculations the effect of electromigration has been included, however, for the processing conditions considered the effect of electromigration is negligible. When the dimensionless quantity $|uI/\sigma_L V| \ll 1$, we expect that electromigration is unimportant. For the parameters used in the tin-bismuth calculations $|uI/\sigma_L V| = 0.021$ and is even smaller for the germanium-gallium calculations. Calculations with $u = 0$ have verified that electromigration is unimportant. For very large currents and small velocities electromigration may be important.

5. Conclusions

We have considered directional solidification of pure materials and binary alloys with a planar crystal-melt interface in the presence of a time-dependent electric current. A variety of numerical results have been presented for growth velocities, thermal fields and solid compositions.

Our results for indium antimonide are in close agreement with the numerical results of Wargo and Witt[13]. For pure bismuth, we have performed calculations for conditions similar to the experiments of Silberstein and Larson[16]. Given the uncertainties in the physical properties and the appropriate far-field boundary conditions, the numerical calculations show reasonable agreement with their experimental results. In our numerical calculations (but not

in the experiments), it is easy to isolate the various thermoelectric effects and this is shown in Figs. (3), (4), (6) and (7).

One of the main uses of electrical pulsing is for interface demarcation in alloys. This technique is based on the change in solute concentration in the solidified material due to the electrical pulse. The calculations for germanium-gallium provide quantitative predictions of the solute composition in the solid due to electrical pulsing, which has been widely used for interface demarcation. Under typical experimental conditions for interface demarcation, the magnitude of the change in solid composition is about five percent of the average solid composition. The calculations for tin-bismuth indicate a similar change in solid composition; however, whether such compositional variations can be observed depends critically on the sensitivity of the observational technique. Apparently etching is an extremely sensitive technique for revealing compositional modulations in the germanium-gallium system.

We have neglected diffusion in the solid, which prevents the consideration of electrical pulses in alloys that would cause melting of the solid. Since the thermal and solutal fields are only coupled at the interface (in the absence of Soret and Dufour effects), it is straightforward to extend our numerical method to treat diffusion in the solid.

Acknowledgments

We thank J. J. Favier, D. J. Larson, Jr., R. J. Schaefer, R. F. Sekerka, M. J. Wargo, A. A. Wheeler, and A. F. Witt for helpful discussions. This research was supported by the Microgravity Sciences and Applications Division of the National Aeronautics and Space

Administration, and the Applied and Computational Mathematics Program at the Defense Advanced Research Projects Agency. One of the authors (LNB) was supported by a National Research Council Postdoctoral Research Fellowship.

Appendix : Linear Theory for a Time Periodic Current

In a reference system moving at velocity V, the set of differential equations governing the unperturbed problem are:

$$\frac{\partial^2 T_S^{(0)}}{\partial z^2} + K_S \frac{\partial T_S^{(0)}}{\partial z} + S_S = 0 \tag{18}$$

$$\frac{\partial^2 T_L^{(0)}}{\partial z^2} + K_L \frac{\partial T_L^{(0)}}{\partial z} + S_L = 0, \text{ and} \tag{19}$$

$$\frac{\partial^2 C_L^{(0)}}{\partial z^2} + \eta \frac{\partial C_L^{(0)}}{\partial z} = 0, \tag{20}$$

in which $S = I_o^2/(\sigma\lambda)$, $K = (c_p V - \tau I_o)/\lambda$, $\eta = (V/D)(1-\alpha_o)$ and $\alpha_o = [uI_o/\sigma V]$. The solutions to the above equations are

$$C_L^{(0)} = \frac{C_{SI}}{1-\alpha_o} + b_c \exp(-\eta z) \tag{21}$$

for the solute, where

$$b_c = \frac{C_{SI}}{1-\alpha_o}\left(\frac{1-k-\alpha_o}{k}\right),$$

and C_{SI} is the composition of the solid phase at the crystal-melt interface. The unperturbed temperatures are

$$T_L^{(0)} = T_M + \left(\frac{mC_{SI}}{k}\right) - (S_L/K_L)z + b_L\left[\exp(-K_L z) - 1\right] \tag{22}$$

$$T_S^{(0)} = T_M + \left(\frac{mC_{SI}}{k}\right) - (S_S/K_S)z + b_S\left[\exp(-K_S z) - 1\right] \tag{23}$$

where

$$b_L = -\left(\frac{G_L + S_L/K_L}{K_L}\right) \text{ and } b_S = -\left(\frac{L_v V + (S_S/K_S)\lambda_S + \lambda_L G_L + \Pi_{SL} I_o}{\lambda_S K_S}\right).$$

and G_L is the unperturbed temperature gradient in the melt at $z = 0$. The perturbed problem is governed by the equations

$$\frac{\partial^2 T_S^{(1)}}{\partial z^2} + K_S \frac{\partial T_S^{(1)}}{\partial z} - i\Omega_L T_S^{(1)} = r_1^S + r_2^S \exp(-K_S z) \tag{24}$$

$$\frac{\partial^2 T_L^{(1)}}{\partial z^2} + K_L \frac{\partial T_L^{(1)}}{\partial z} - i\Omega_L T_L^{(1)} = r_1^L + r_2^L \exp(-K_L z) \text{ and} \tag{25}$$

$$\frac{\partial^2 C_L^{(1)}}{\partial z^2} + \eta \frac{\partial C_L^{(1)}}{\partial z} - \frac{i\omega}{D} C_L^{(1)} = r^C \exp(-\eta z), \tag{26}$$

in which

$$\Omega = \frac{\omega c_p}{\lambda} \tag{27}$$

$$r_1 = \frac{I_1}{\lambda}\left(-\frac{2I_0}{\sigma} - \frac{\tau S}{K}\right),$$

$$r_2 = \frac{-I_1 \tau K b}{\lambda} \text{ and}$$

$$r^C = \frac{-u I_1 \eta b_c}{\sigma_L D}.$$

The solutions to the perturbed set of equations (24) to (24) are

$$T^{(1)} = a_1 \exp(\Upsilon_+ z) + a_2 \exp(\Upsilon_- z) - \frac{r_1 + r_2 \exp(-Kz)}{i\Omega} \tag{28}$$

for either of the thermal fields, and

$$C^{(1)} = a_1^c \exp(\Phi_+ z) + a_2^c \exp(\Phi_- z) - \frac{r^C D \exp(-\eta z)}{i\omega} \tag{29}$$

where,

$$\Upsilon_\pm = -\frac{K}{2} \pm \left[\left(\frac{K}{2}\right)^2 + i\Omega\right]^{1/2} \text{ and}$$

$$\Phi_\pm = -\frac{\eta}{2} \pm \left[\left(\frac{\eta}{2}\right)^2 + \frac{i\omega}{D}\right]^{1/2}.$$

The four interfacial boundary conditions, (4) - (7), are linearized, and yield

$$a_1^S + a_2^S + \delta\left[m\eta b_c - (S_S/K_S + b_S K_S)\right] = \frac{r_1^S + r_2^S}{i\Omega_S} + m\left(a_1^C + a_2^C - \frac{r^C D_L}{i\omega}\right) \tag{30}$$

$$a_1^L + a_2^L + \delta\left[m\eta b_C - (S_L/K_L + b_L K_L)\right] = \frac{r_1^L + r_2^L}{i\Omega_L} + m\left(a_1^C + a_2^C - \frac{r^C D_L}{i\omega}\right) \tag{31}$$

$$a_1^C\left[\Phi_+ + \eta - \frac{Vk}{D}\right] + a_2^C\left[\Phi_- + \eta - \frac{Vk}{D}\right] + \delta\left[\frac{Vk\eta b_c}{D_L} + \frac{i\omega(1-k)C_{SI}}{kD_L}\right] \tag{32}$$
$$= \frac{-r^C Vk}{i\omega} + \left(\frac{uI_1 C_{SI}}{\sigma D_L k}\right)$$

$$a_1^S\left[\lambda_S \Upsilon_+^S\right] + a_2^S\left[\lambda_S \Upsilon_-^S\right] + a_1^L\left[-\lambda_L \Upsilon_+^L\right] + a_2^L\left[-\lambda_L \Upsilon_-^L\right] + \tag{33}$$
$$\delta\left[\lambda_S (K_S)^2 b_S - \lambda_L (K_L)^2 b_L - i\omega L_v\right] = \Pi_{SL} I_1 - \frac{\lambda_S r_2^S K_S}{i\Omega_S} + \frac{\lambda_L r_2^L K_L}{i\Omega_L}$$

for the perturbed problem. The far-field conditions for the perturbed quantities are of the form

$$A^\infty \frac{\partial T^{(1)}}{\partial z} + B^\infty T^{(1)} = 0. \tag{34}$$

The four interface conditions plus the three far-field conditions for $T_L^{(1)}$, $T_S^{(1)}$ and $C^{(1)}$ form a set of seven linear inhomogeneous equations for the seven unknowns, a_1^S, a_1^L, a_2^S, a_2^L, a_1^c, a_2^c and δ. These linear equations are solved numerically, and values of the perturbed quantities are calculated.

References

[1] William G. Pfann, Zone Melting (John Wiley, New York, 1966).

[2] J. M. Bardeen and B. S. Chandrasekhar, J. Appl. Phys., 29 (1958) 1372.

[3] J. D. Verhoeven, Trans. Met. Soc. AIME, 239 (1967) 694.

[4] J. C. Warner and J. D. Verhoeven, Met. Trans., 4 (1973) 1255.

[5] T. Bryskiewicz, C. F. Boucher, Jr., J. Lagowski and H. C. Gatos, J. Crystal Growth 82 (1987) 279.

[6] A. Okamoto, J. Lagowski and H. C. Gatos, J. Appl. Phys. 53 (1982) 1706.

[7] D. J. Wollkind and S. Wang, SIAM J. Appl. Math 48 (1988) 52.

[8] A. A. Wheeler, S. R. Coriell, G. B. McFadden and D. T. J. Hurle, J. Crystal Growth 88 (1988) 1.

[9] S. R. Coriell, G. B. McFadden, A. A. Wheeler and D. T. J. Hurle, J. Crystal Growth 94 (1989) 334.

[10] R. Singh and A. F. Witt and H. C. Gatos, J. Electrochem. Soc. 115 (1968) 112.

[11] D. E. Holmes and H. C. Gatos, J. Appl. Phys., 52 (1981) 2971.

[12] M. J. Wargo and A. F. Witt, J. Crystal Growth 66 (1984), 289.

[13] M. J. Wargo and A. F. Witt, J. Crystal Growth 66 (1984), 541.

[14] T. Duffar et al., to be published.

[15] R. P. Silberstein, D. J. Larson, Jr., and B. Dressler, Met Trans 15A (1984) 2147.

[16] R. P. Silberstein and D. J. Larson, Jr., Mat. Res. Soc. Symp. Proc. 87, (1987) 129.

[17] J. J. Derby and R. A. Brown, Chem. Eng. Sci. 41 (1986) 37.

[18] D. Kahaner, C. Moler and S. Nash, Numerical Methods and Software (Prentice Hall, Englewood Cliffs, NJ, 1989).

[19] V. G. Smith and W. A. Tiller and J. W. Rutter, Canadian Journal of Physics, 33 (1955) 723.

[20] W. A. Tiller and R. F. Sekerka, J. Appl. Phys., 35 (1964) 2726.

[21] J. J. Favier and A. Rouzaud, Adv. Space Res. 6 (1986) 111.

[22] A. R. Ubbelohde, Proc. Roy. Soc. (London) A293 (1966) 291.

Table 1: Comparisons of the solute transient given by Smith et al.[19] with the numerical calculations for $m = 0$. The data is for Ge-Ga with $V = 0.019$ cm/s so that $D/V = .01$ cm and the cutoff length is given by $L_C = 4D/V = 0.04$ cm. The initial solutal field has a uniform value of unity. N is the number of intervals used to discretize the liquid domain.

t(secs)	Analytical	Analytical – Numerical		
	C_L	$N = 50$	$N = 100$	$N = 200$
.02	1.21563	0.00488	0.00121	0.00030
.04	1.31366	0.00461	0.00116	0.00029
.06	1.39238	0.00462	0.00116	0.00029
.08	1.46112	0.00471	0.00118	0.00029
.10	1.52350	0.00485	0.00122	0.00030
.12	1.58136	0.00501	0.00126	0.00032
.14	1.63579	0.00518	0.00130	0.00033
.16	1.68750	0.00535	0.00134	0.00034
.18	1.73699	0.00553	0.00139	0.00035
.20	1.78462	0.00570	0.00143	0.00036

Table 2: Comparisons of the solute transient given by Smith et al.[19] with the numerical calculations for the case in which $m = 0$. The interface is initially travelling at the constant velocity V_1, and the interface velocity is instantaneously doubled at $t = 0$. The interface composition increases and then settles down into a steady state profile. Comparison of the analytical solution is made with numerical calculations for different mesh spacings. The data is for an alloy of Ge-Ga with an initial velocity $V_1 = 0.0019$ cm/s so that $D/V_1 = 0.1$ cm. The cutoff length is given by $L_C = 4D/V_1 = 0.4$ cm.

t(secs)	Analytical	Analytical – Numerical		
		$N = 50$	$N = 100$	$N = 200$
.02	1.03284	0.00610	0.00141	0.00035
2.0	1.08996	0.00351	0.00088	0.00022
4.0	1.11509	0.00351	0.00088	0.00022
6.0	1.12962	0.00364	0.00091	0.00023
8.0	1.13880	0.00379	0.00095	0.00024
10.0	1.14468	0.00394	0.00099	0.00025
12.0	1.14831	0.00408	0.00102	0.00025
14.0	1.15034	0.00422	0.00106	0.00027
16.0	1.15116	0.00434	0.00109	0.00027
18.0	1.15107	0.00446	0.00112	0.00028
20.0	1.15027	0.00458	0.00115	0.00029
30.0	1.13994	0.00507	0.00129	0.00034

Table 3: Comparison of the analytical amplitude of the oscillatory component $\omega\delta$ of the interface velocity with the maximum and minimum values of the numerically-determined oscillatory component of the interface velocity for a current of the form $I = I_1 \exp(i\omega t)$, with $\omega = 2\pi$ x 10^{-2}. The analytical results are calculated from the linear theory derived in the Appendix. The numerical results are determined after significant decay of the initial transient. The temperature and the composition are fixed at the outer boundaries. The thermal sample length is 0.5 cm for both the solid and liquid, and the solutal cutoff length is a distance D/V away from the interface in the melt, with $V = 38\mu$m/s. The material parameters are for germanium-gallium alloys listed in Table (4).

I_1	Anal. (mag.)	Num. (max)	Num. (min)
0.1	9.802 x 10^{-7}	9.993 x 10^{-7}	-9.994 x 10^{-7}
1.0	9.802 x 10^{-6}	9.997 x 10^{-6}	-9.999 x 10^{-6}
10.0	9.802 x 10^{-5}	9.521 x 10^{-5}	-9.854 x 10^{-5}

Table 4: Thermophysical Properties

Property	Sn-Bi	Ge-Ga	Bi	InSb
$c_{pL}[J/(cm^3K)]$	1.0	2.1	1.46	1.53
$c_{pS}[J/(cm^3K)]$	1.0	2.1	1.46	1.4
$T_M[K]$	505	1209	549	803
$L[J/cm^3]$	410	2520	54.0	1350
$\lambda_L[J/(cmKs)]$	0.3	0.7	0.124	0.13
$\lambda_S[J/(cmKs)]$	0.6	0.24	0.065	0.046
$\sigma_L[1/(\Omega cm)]$	2.1×10^4	1.6×10^4	7.8×10^3	9.5×10^3
$\sigma_S[1/(\Omega cm)]$	4.5×10^4	1.25×10^3	3.8×10^3	2.9×10^3
$\tau_S[V/K]$	-5.7×10^{-7}	0.0	7.62×10^{-5}	-4.0×10^{-5}
$\tau_L[V/K]$	0.0	-2.7×10^{-4}	-7.13×10^{-7}	-4.0×10^{-5}
$\Pi_{SL}[V]$	-6.1×10^{-4}	-9.7×10^{-2}	-0.014	-9.7×10^{-2}
$D[cm^2/s]$	1.8×10^{-5}	1.9×10^{-4}	1.9×10^{-4}	1.9×10^{-4}
$m[at.\%/K]$	-2.9	-3.7		
k	0.3	0.086		
$u[cm^2/(Vs)]$	-1.5×10^{-3}	3.6×10^{-3}		

Figure Captions

Figure 1 : Plot of the interfacial growth velocity as a function of time for pure $InSb$. The upper plot shows calculations for the case of $1s$ current pulses of $20.3A/cm^2$ applied at times $3s$ and $7s$. The bottom plot shows the case of repeated current pulses of $9.5A/cm^2$ which are on for $20s$ and off for $40s$. The initial temperature gradient in the melt at the interface is $25.0K/cm$ in both cases.

Figure 2 : The change in temperature and the interface velocity as a function of time for pure Bi, with a current pulse of $80A/cm^2$ and duration $10s$. The temperature changes are measured at three fixed positions in the liquid, 0.05 (lower curve), 1.25 (middle curve) and $2.27cm$ (upper curve) from the initial interface. The initial change in temperature is zero, but the middle and upper curves have been offset by 5 and $10K$, respectively. The triangles mark the beginning and the end of the current pulse. All thermoelectric effects are included.

Figure 3 : The contributions of the Peltier, Thomson and Joule effects to the change in temperature as a function of time for pure Bi, with a current pulse of $80A/cm^2$ and duration $10s$. The temperature changes are measured at three fixed positions in the liquid, 0.05 (lower curve), 1.25 (middle curve) and $2.27cm$ (upper curve) from the initial interface. The initial change in temperature is zero, but the middle and upper curves have been offset by 5 and $10K$, respectively. The triangles mark the beginning and the end of the current pulse. In each plot, the thermoelectric effects other than

the one considered are set to zero.

Figure 4 : The contributions of the Peltier, Thomson and Joule effects to the interface velocity as a function of time for pure Bi, with a current pulse of $80A/cm^2$ and duration $10s$. The triangles mark the beginning and the end of the current pulse. In each plot, the thermoelectric effects other than the one considered are set to zero.

Figure 5 : The change in temperature and the interface velocity as a function of time for pure Bi, with a current pulse of $-80A/cm^2$ and duration $10s$. The temperature changes are measured at three fixed positions in the liquid, 0.05 (lower curve), 1.25 (middle curve) and $2.27cm$ (upper curve) from the initial interface. The initial change in temperature is zero, but the middle and upper curves have been offset by 5 and $10K$, respectively. The triangles mark the beginning and the end of the current pulse. All thermoelectric effects are included.

Figure 6 : The contributions of the Peltier, Thomson and Joule effects to the change in temperature as a function of time for pure Bi, with a current pulse of $-80A/cm^2$ and duration $10s$. The temperature changes are measured at three fixed positions in the liquid, 0.05 (lower curve), 1.25 (middle curve) and $2.27cm$ (upper curve) from the initial interface. The initial change in temperature is zero, but the middle and upper curves have been offset by 5 and $10K$, respectively. The triangles mark the beginning and the end of the current pulse. In each plot, the thermoelectric effects other than the one considered are set to zero.

Figure 7 : The contributions of the Peltier, Thomson and Joule effects to the interface velocity as a function of time for pure Bi, with a current pulse of $-80A/cm^2$ and duration $10s$. The triangles mark the beginning and the end of the current pulse. In each plot, the thermoelectric effects other than the one considered are set to zero.

Figure 8 : The change in temperature and the interface velocity as a function of time, and the solid gallium concentration as a function of position for an alloy of germanium containing 0.1 at% gallium. A current of 25 A/cm^2 is applied at $t = 10s$. The temperature changes are measured at three fixed positions in the liquid, 0.02 (lower curve), 0.5 (middle curve) and $0.91cm$ (upper curve) from the initial interface. The initial change in temperature is zero, but the middle and upper curves have been offset by 0.1 and $0.2K$, respectively.

Figure 9 : The change in temperature and the interface velocity as a function of time, and the solid gallium concentration as a function of position for an alloy of germanium containing 0.1 at% gallium. A current of $-25A/cm^2$ is applied at $t = 10s$. The temperature changes are measured at three fixed positions in the liquid, 0.02 (lower curve), 0.5 (middle curve) and $0.91cm$ (upper curve) from the initial interface. The initial change in temperature is zero, but the middle and upper curves have been offset by 0.3 and $0.6K$, respectively.

Figure 10: The change in temperature as a function of time in pure germanium and in the germanium alloys with 0.3 and 0.5 at% gallium. At $t = 10s$, a current of 25 A/cm^2 is applied. The changes in temperature are calculated at distances of 0.02 cm. (lower

curve), 0.5 cm. (middle curve) and 0.91 cm. (upper curve) from the initial interface position, in a moving reference system. The curves are offset for clarity.

Figure 11: The change in temperature as a function of time in pure germanium and in the germanium alloys with 0.3 and 0.5 at% gallium. At $t = 10s$, a current of $-25A/cm^2$ is applied. The changes in temperature are calculated at distances of 0.02 cm. (lower curve), 0.5 cm. (middle curve) and 0.91 cm. (upper curve) from the initial interface position, in a moving reference system. The curves are offset for clarity.

Figure 12: The change in temperature and the interface velocity as a function of time, and the solid gallium concentration as a function of position for an alloy of germanium containing 0.1 at% gallium. A current pulse of $80A/cm^2$ is applied for 0.1 s. The temperature changes are measured at three fixed positions in the liquid, 0.02 (lower curve), 0.5 (middle curve) and $0.91cm$ (upper curve) from the initial interface, in a moving reference system. The curves are offset for clarity.

Figure 13: The change in temperature and the interface velocity as a function of time, and the solid gallium concentration as a function of position for an alloy of germanium containing 0.1 at% gallium. A current pulse of $-80A/cm^2$ is applied for 0.1 s. The temperature changes are measured at three fixed positions in the liquid, 0.02 (lower curve), 0.5 (middle curve) and $0.91cm$ (upper curve) from the initial interface, in a moving reference system. The curves are offset for clarity.

Figure 14: The change in temperature and the interface velocity as a function of time, and

the solid bismuth concentration as a function of position for an alloy of tin containing 0.78 at% bismuth. A current pulse of $50A/cm^2$ is applied for 5.0 s. The temperature changes are measured at three fixed positions in the liquid, 0.03 (lower curve), 0.75 (middle curve) and $1.36cm$ (upper curve) from the initial interface, in a moving reference system. The curves are offset for clarity.

Figure 15: The change in temperature and the interface velocity as a function of time, and the solid bismuth concentration as a function of position for an alloy of tin containing 0.78 at% bismuth. A current pulse of $-50A/cm^2$ is applied for 5.0 s. The temperature changes are measured at three fixed positions in the liquid, 0.03 (lower curve), 0.75 (middle curve) and $1.36cm$ (upper curve) from the initial interface, in a moving reference system. The curves are offset for clarity.

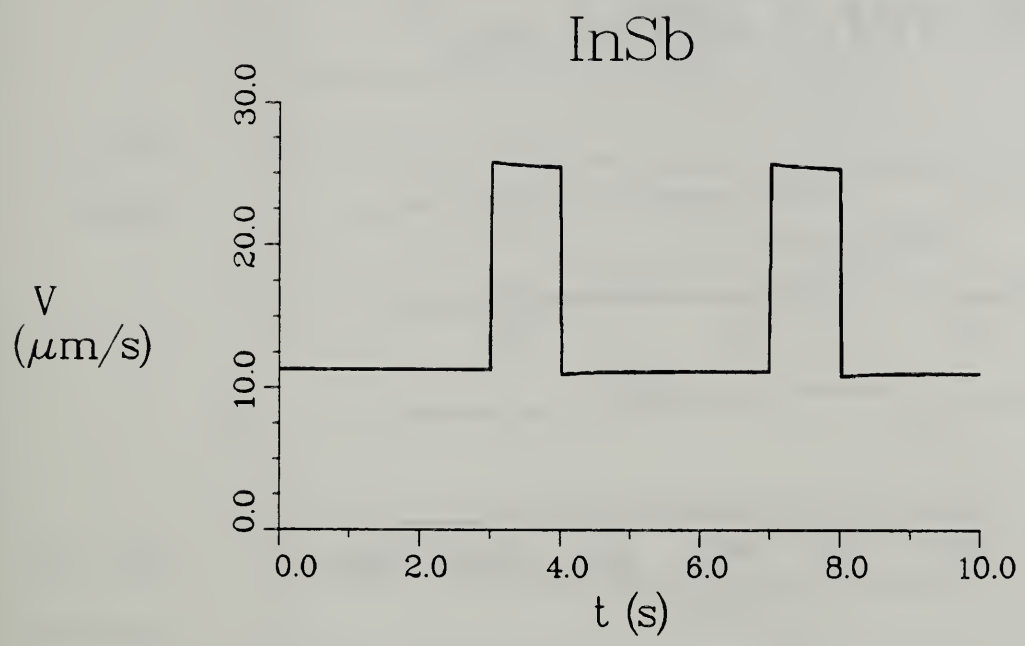
InSb
V
(μm/s)
30.0
20.0
10.0
0.0
0.0
2.0
4.0
6.0
8.0
10.0
t (s)

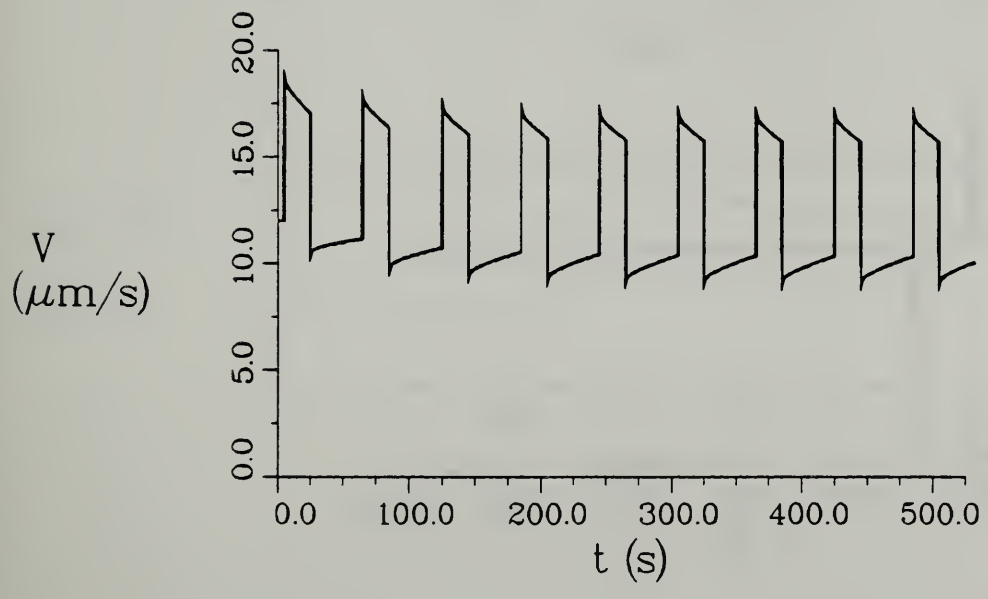
V
(μm/s)
20.0
15.0
10.0
5.0
0.0
0.0
100.0
200.0
300.0
400.0
500.0
t (s)

Figure 1

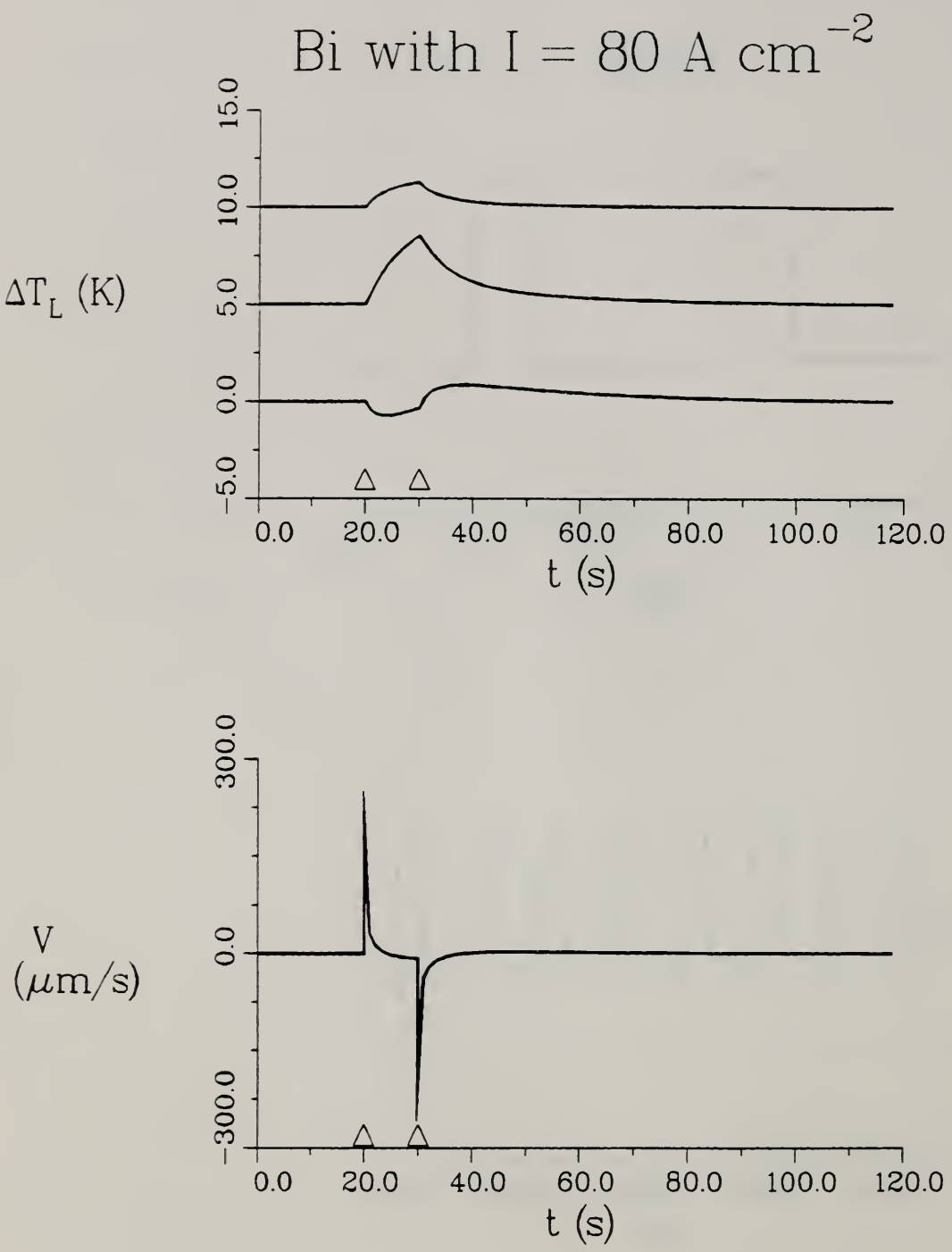
Bi with I = 80 A cm^{-2}
ΔT_L (K)
15.0
10.0
5.0
0.0
−5.0
0.0
20.0
40.0
60.0
80.0
100.0
120.0
t (s)
V
(μm/s)
300.0
0.0
−300.0
0.0
20.0
40.0
60.0
80.0
100.0
120.0
t (s)

Figure 2

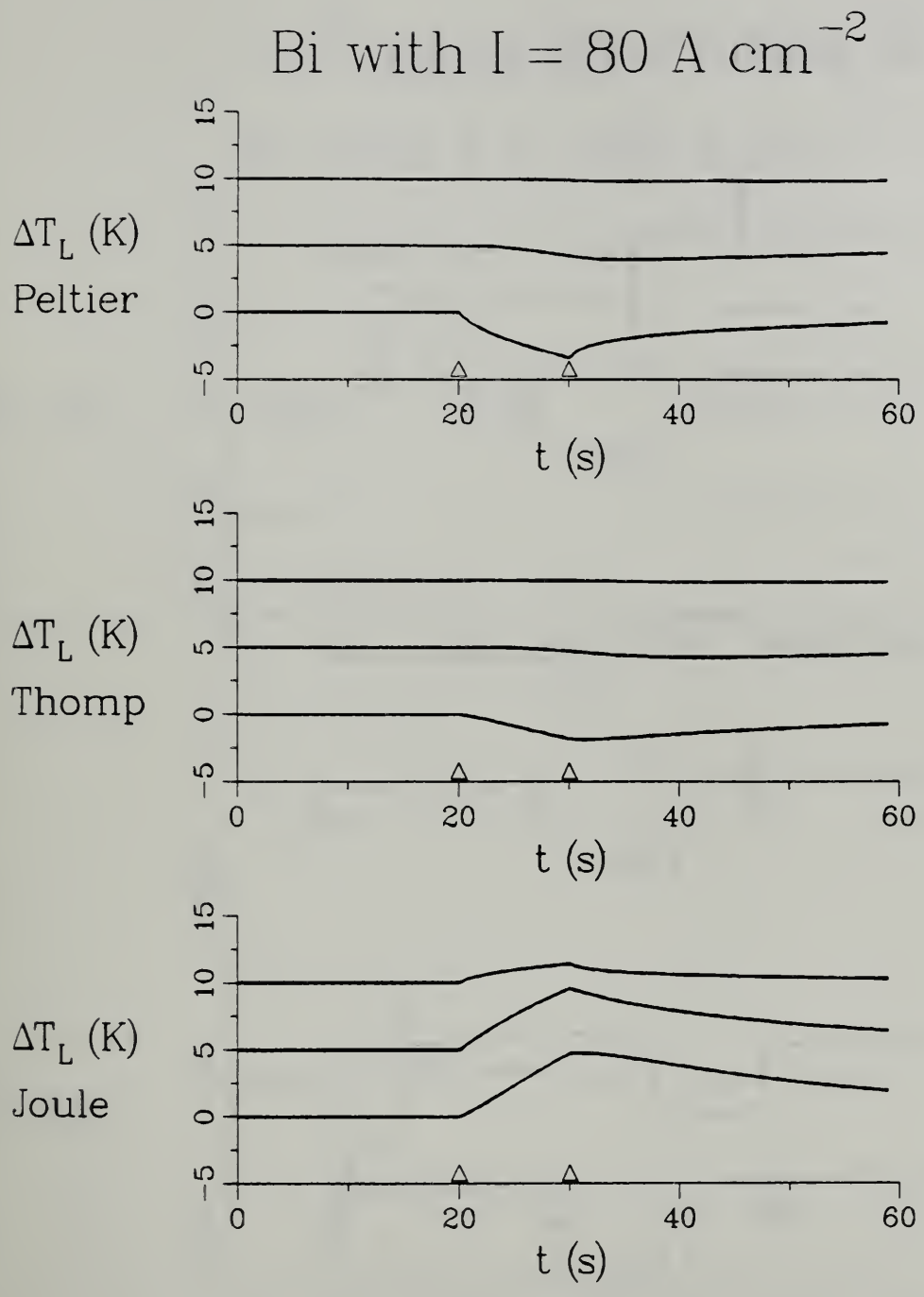
Bi with I = 80 A cm^{-2}
ΔT_L (K)
Peltier
15
10
5
0
−5
0
20
40
60
t (s)
ΔT_L (K)
Thomp
15
10
5
0
−5
0
20
40
60
t (s)
ΔT_L (K)
Joule
15
10
5
0
−5
0
20
40
60
t (s)

Figure 3

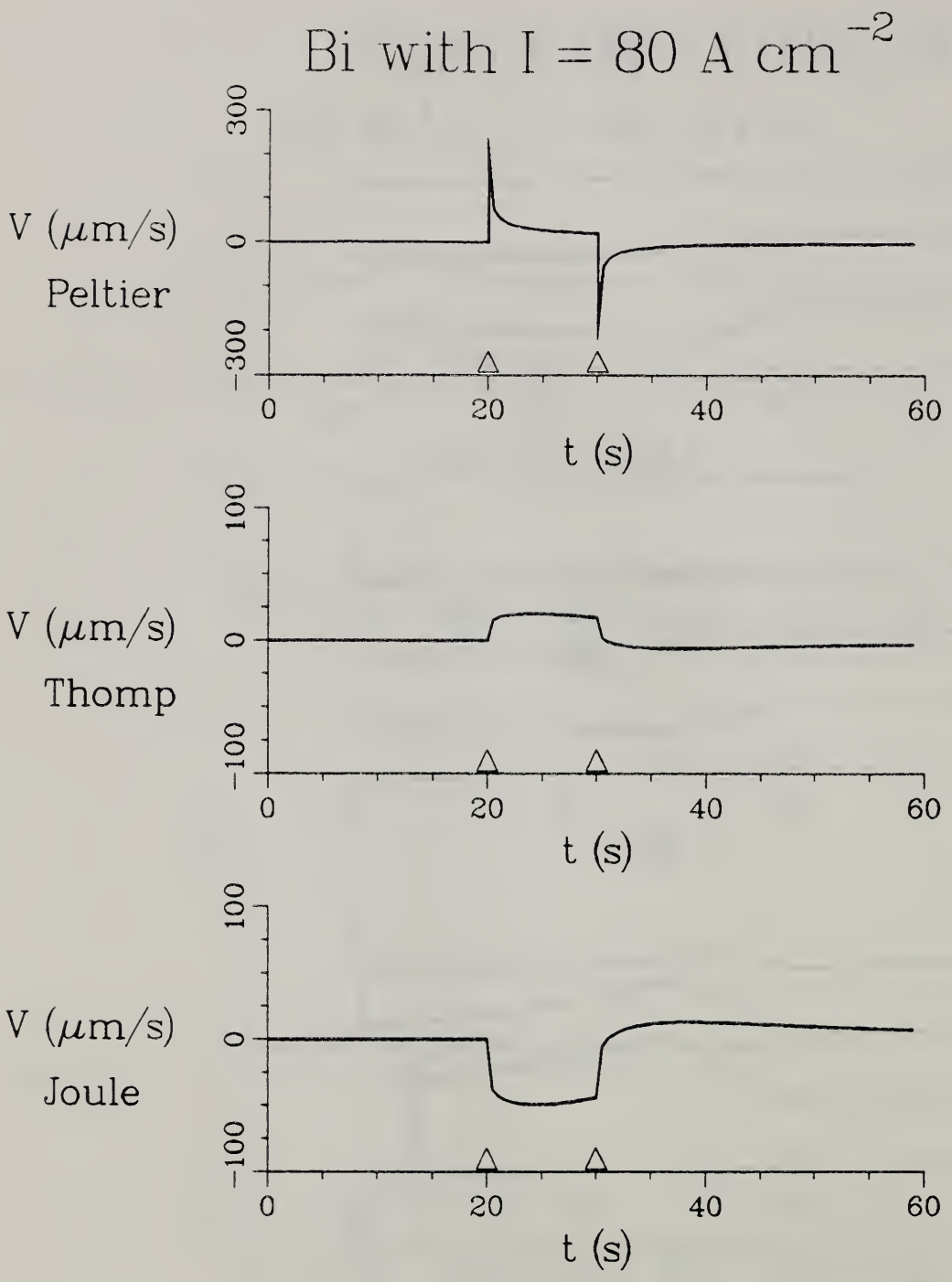
Bi with I = 80 A cm^{-2}
V (μm/s)
Peltier
300
0
−300
0
20
40
60
t (s)
V (μm/s)
Thomp
100
0
−100
0
20
40
60
t (s)
V (μm/s)
Joule
100
0
−100
0
20
40
60
t (s)

Figure 4

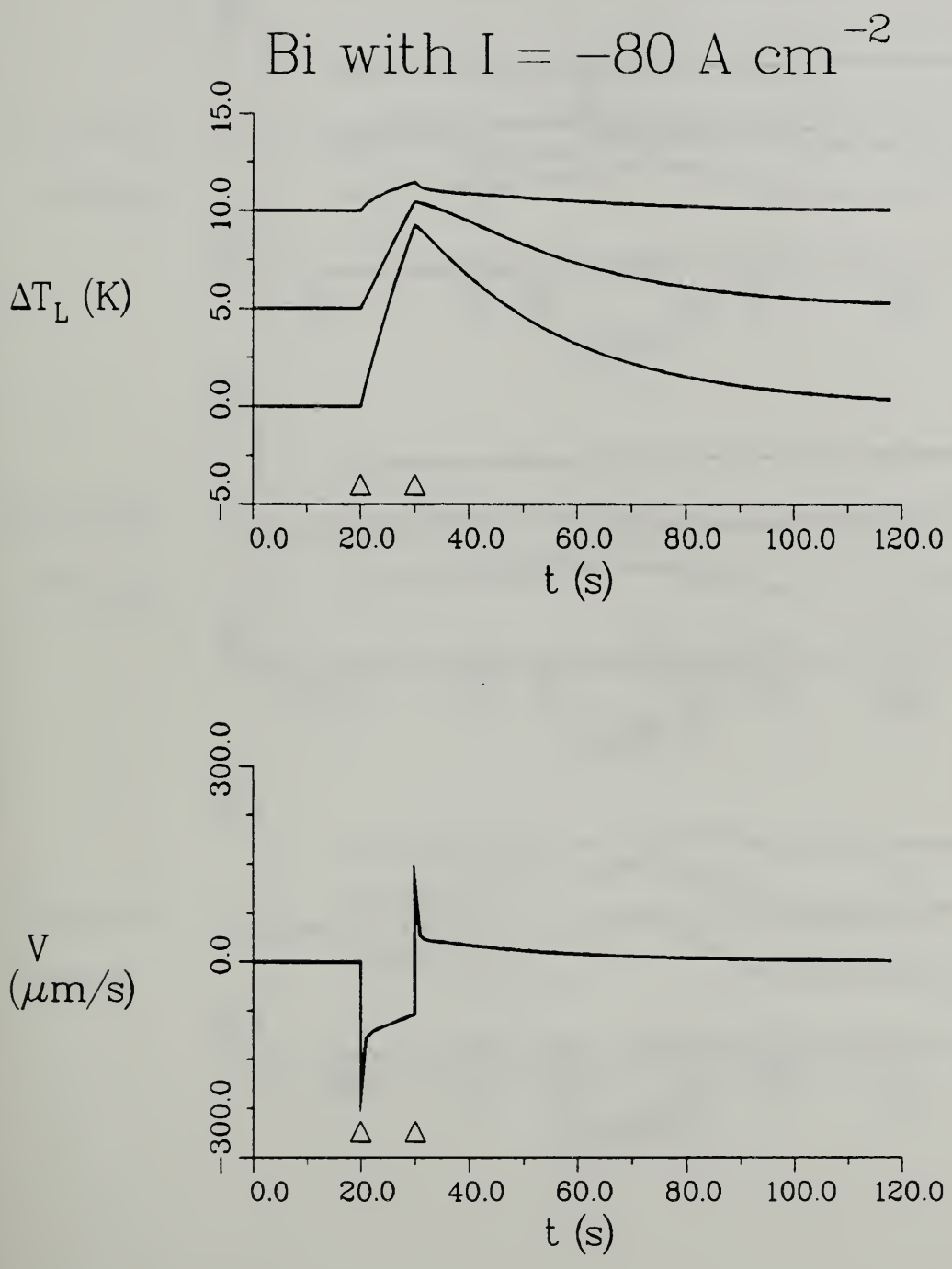
Bi with I = −80 A cm^{-2}
ΔT_L (K)
15.0
10.0
5.0
0.0
−5.0
0.0
20.0
40.0
60.0
80.0
100.0
120.0
t (s)
V
(μm/s)
300.0
0.0
−300.0
0.0
20.0
40.0
60.0
80.0
100.0
120.0
t (s)

Figure 5

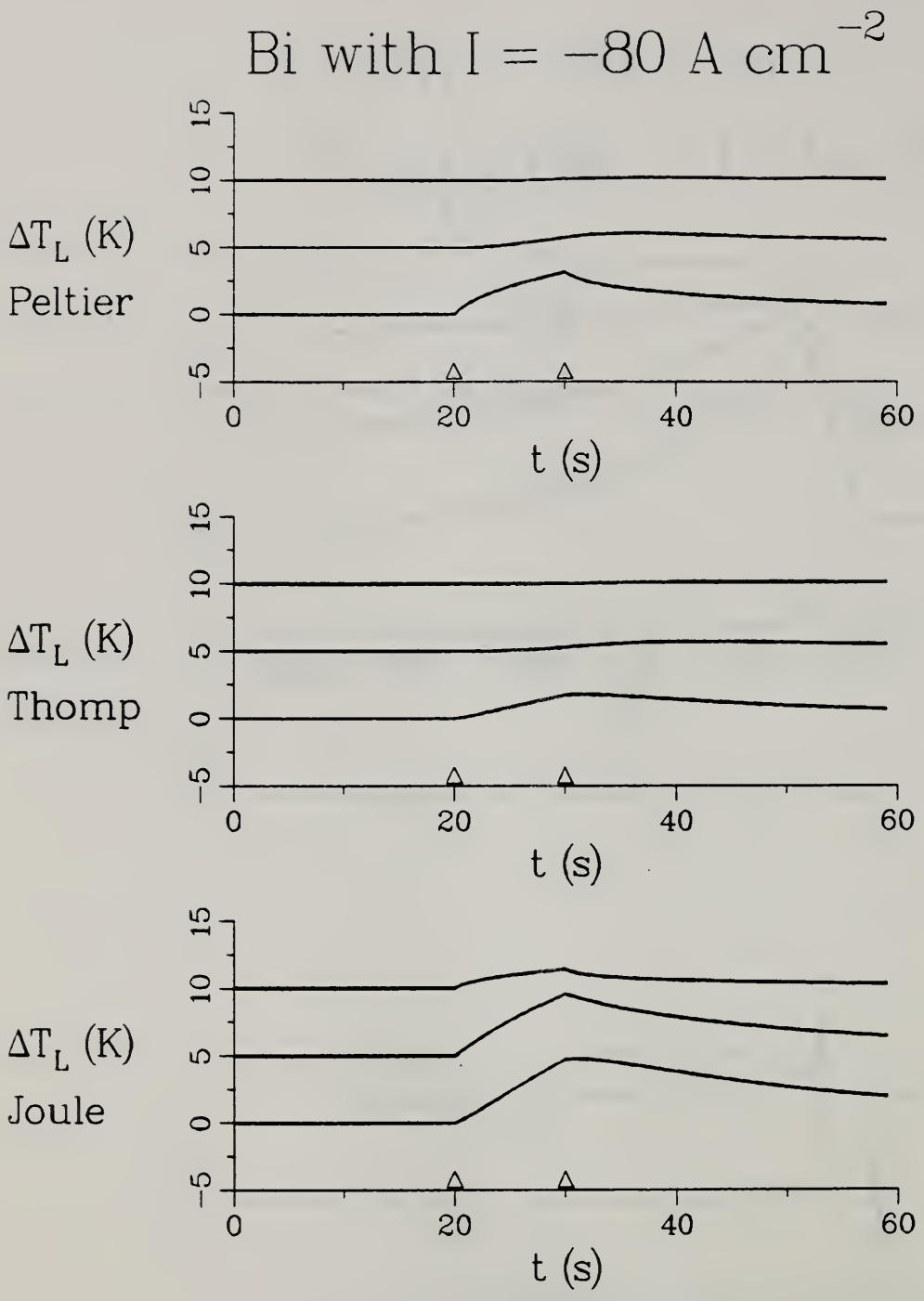
Bi with I = −80 A cm^{-2}
ΔT_L (K)
Peltier
15
10
5
0
−5
0
20
40
60
t (s)
ΔT_L (K)
Thomp
15
10
5
0
−5
0
20
40
60
t (s)
ΔT_L (K)
Joule
15
10
5
0
−5
0
20
40
60
t (s)

Figure 6

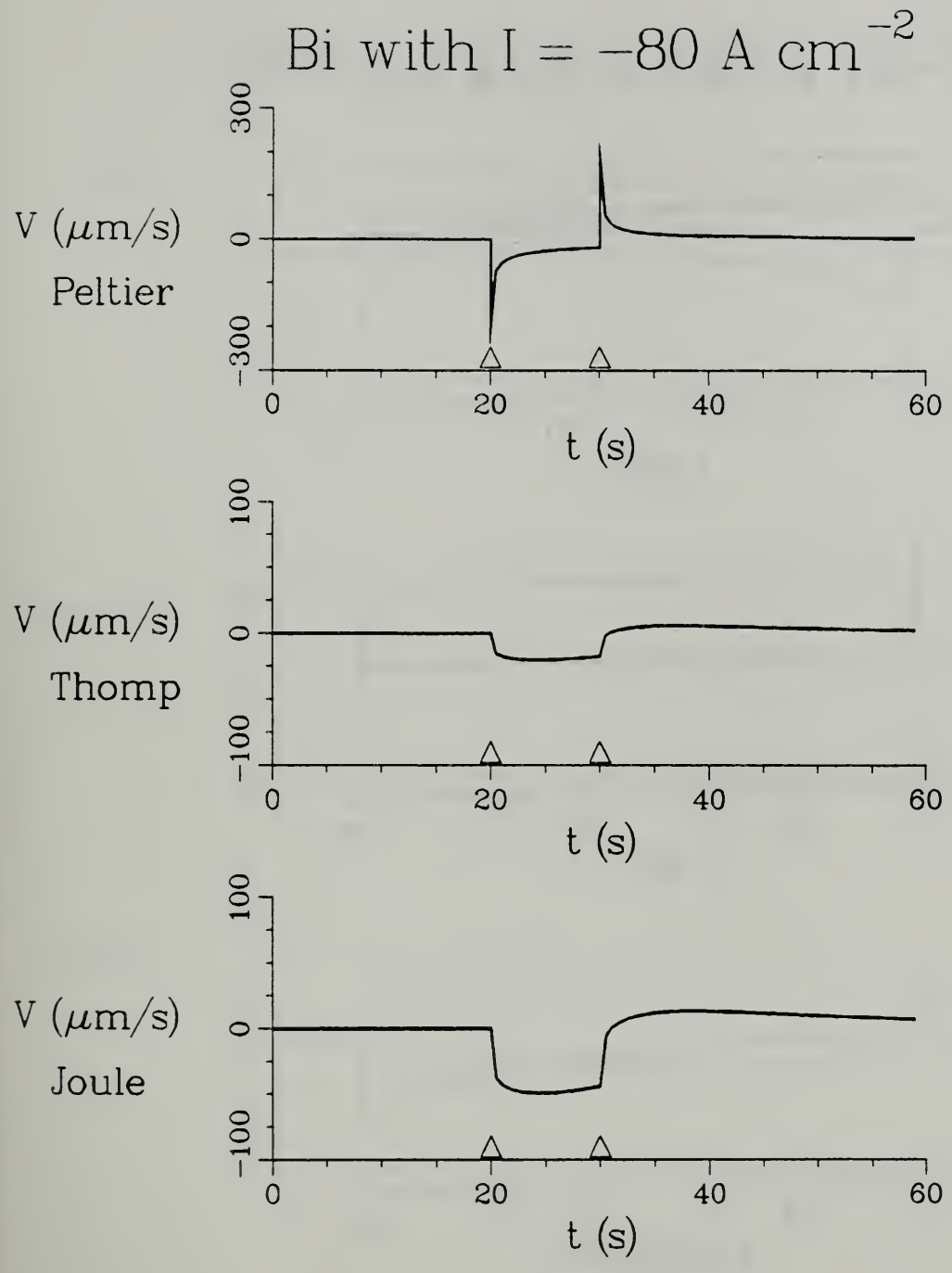
Bi with I = −80 A cm^{-2}
V (μm/s)
Peltier
300
0
−300
0
20
40
60
t (s)
V (μm/s)
Thomp
100
0
−100
0
20
40
60
t (s)
V (μm/s)
Joule
100
0
−100
0
20
40
60
t (s)

Figure 7

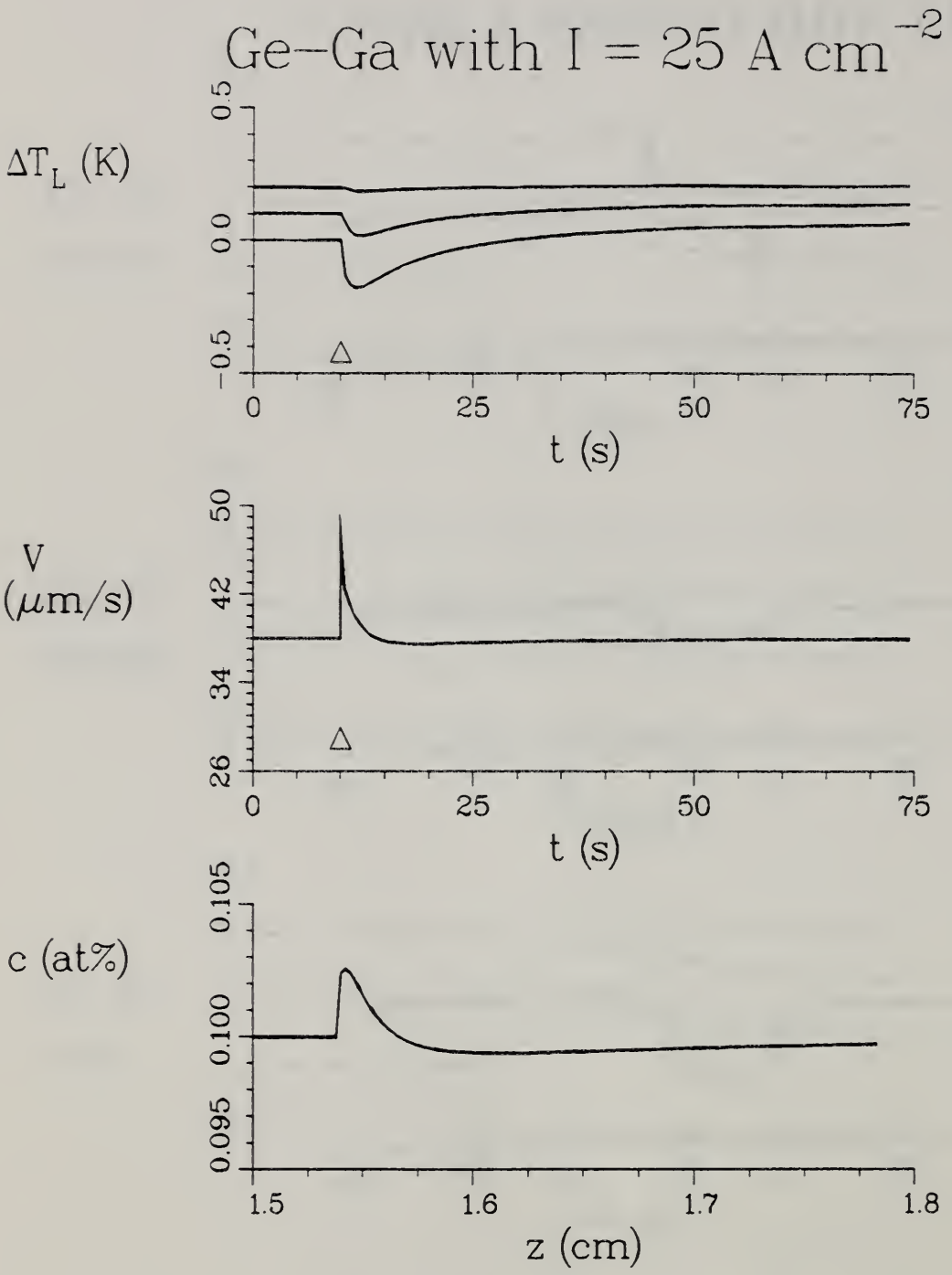
Ge–Ga with I = 25 A cm^{-2}
ΔT_L (K)
0.5
0.0
−0.5
Δ
0
25
50
75
t (s)
V
(μm/s)
50
42
34
26
Δ
0
25
50
75
t (s)
c (at%)
0.105
0.100
0.095
1.5
1.6
1.7
1.8
z (cm)

Figure 8

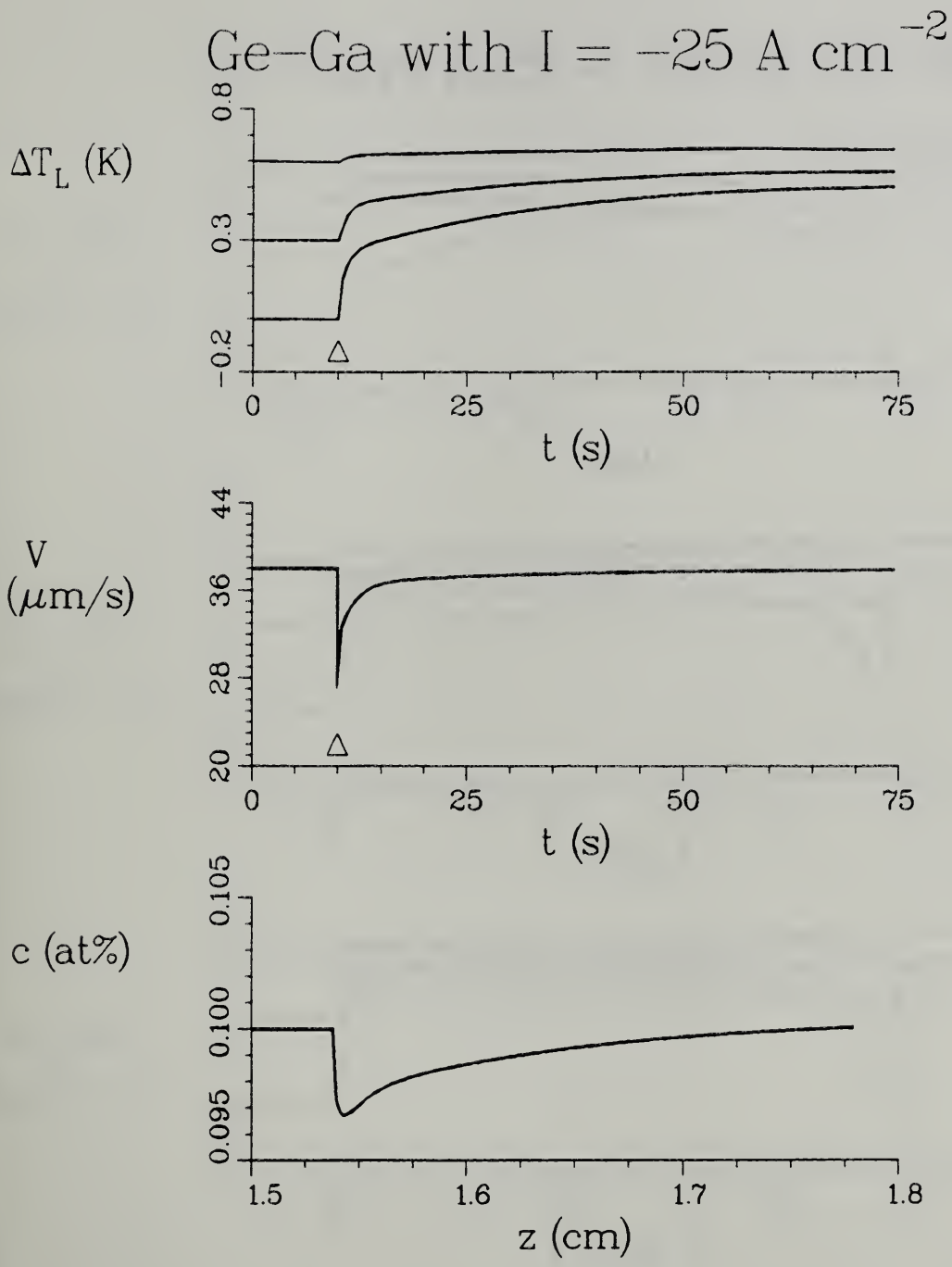
Ge–Ga with I = –25 A cm^{-2}
ΔT_L (K)
0.8
0.3
–0.2
0
25
50
75
t (s)
V
(μm/s)
44
36
28
20
0
25
50
75
t (s)
c (at%)
0.105
0.100
0.095
1.5
1.6
1.7
1.8
z (cm)

Figure 9

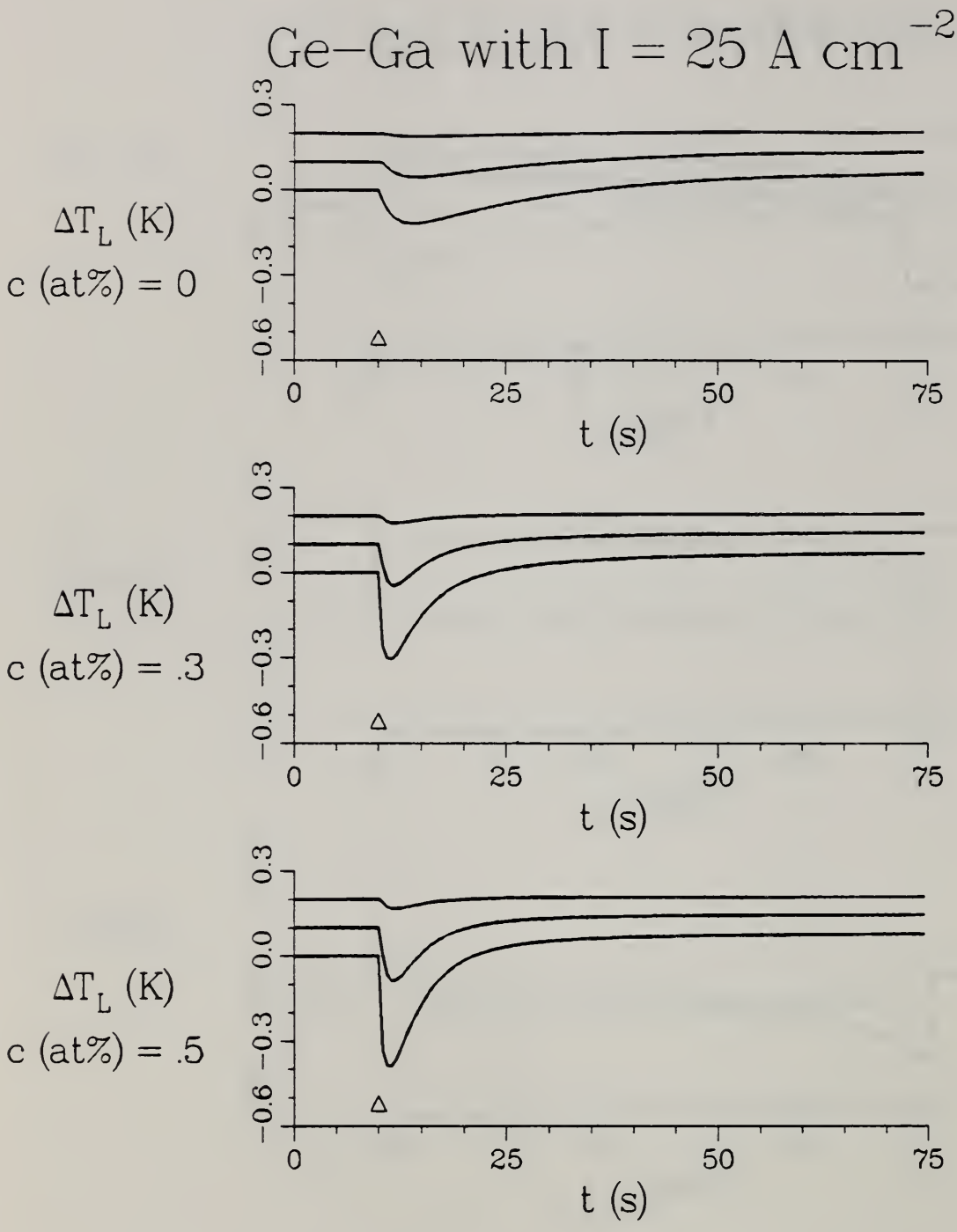
Ge–Ga with I = 25 A cm^{-2}
ΔT_L (K)
c (at%) = 0
ΔT_L (K)
c (at%) = .3
ΔT_L (K)
c (at%) = .5
0.3
0.0
−0.3
−0.6
0
25
50
75
t (s)
Δ

Figure 10

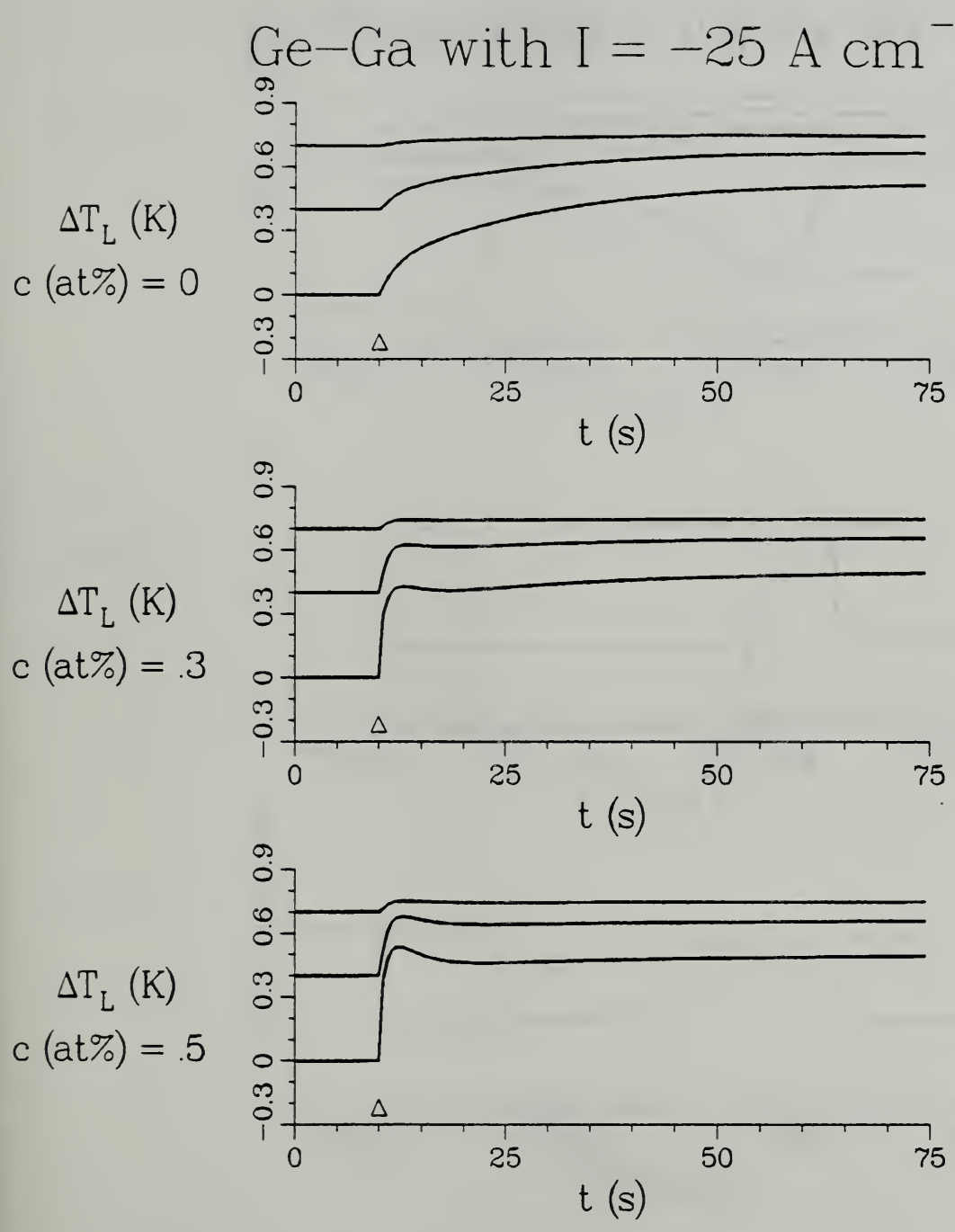
Ge–Ga with I = –25 A cm^{-2}
ΔT_L (K)
c (at%) = 0
ΔT_L (K)
c (at%) = .3
ΔT_L (K)
c (at%) = .5
0.9
0.6
0.3
0
–0.3
Δ
0
25
50
75
t (s)

Figure 11

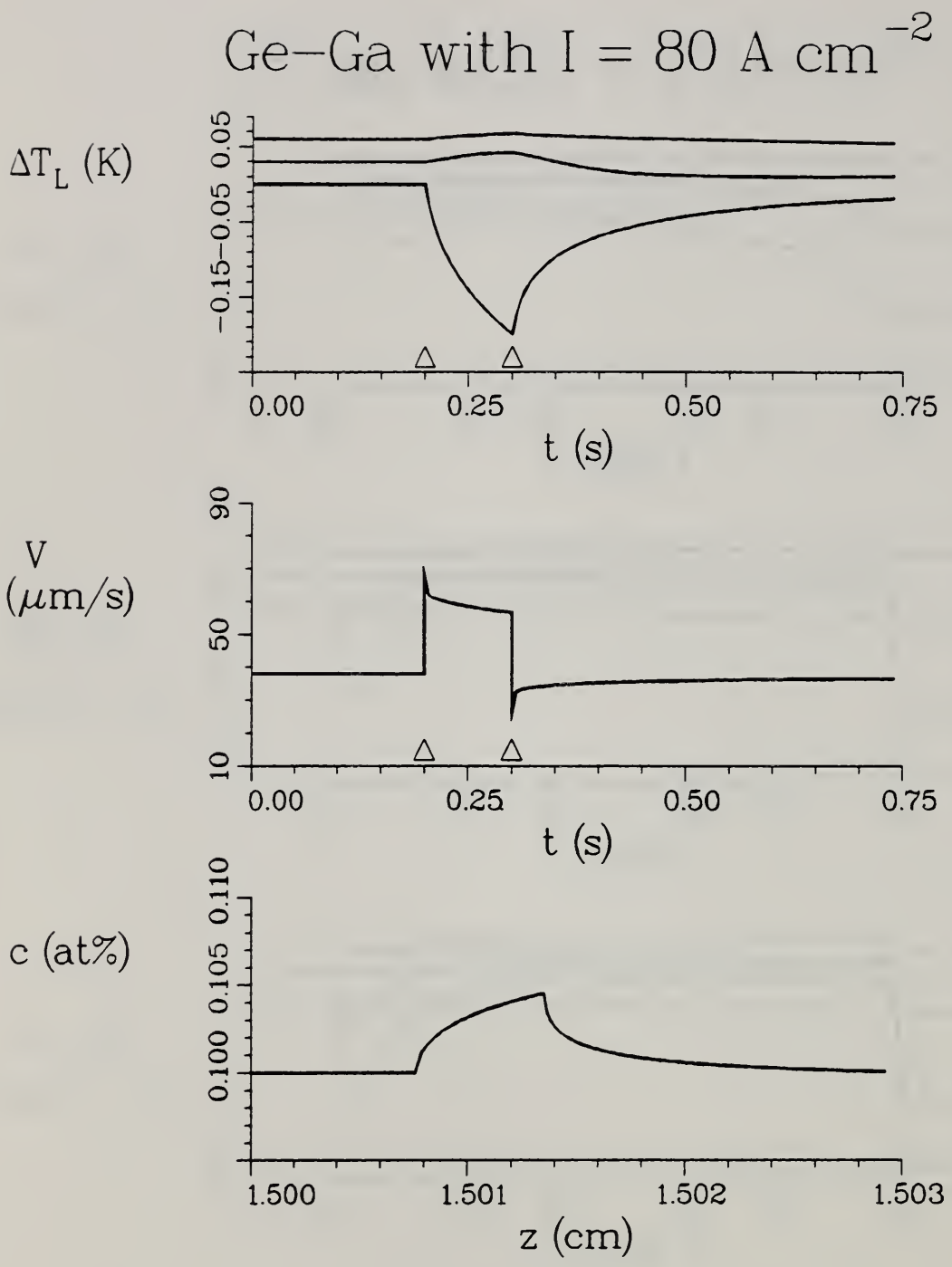
Ge–Ga with I = 80 A cm^{-2}
ΔT_L (K)
0.05
−0.05
−0.15
0.00
0.25
0.50
0.75
t (s)
V
(μm/s)
90
50
10
0.00
0.25
0.50
0.75
t (s)
c (at%)
0.110
0.105
0.100
1.500
1.501
1.502
1.503
z (cm)

Figure 12

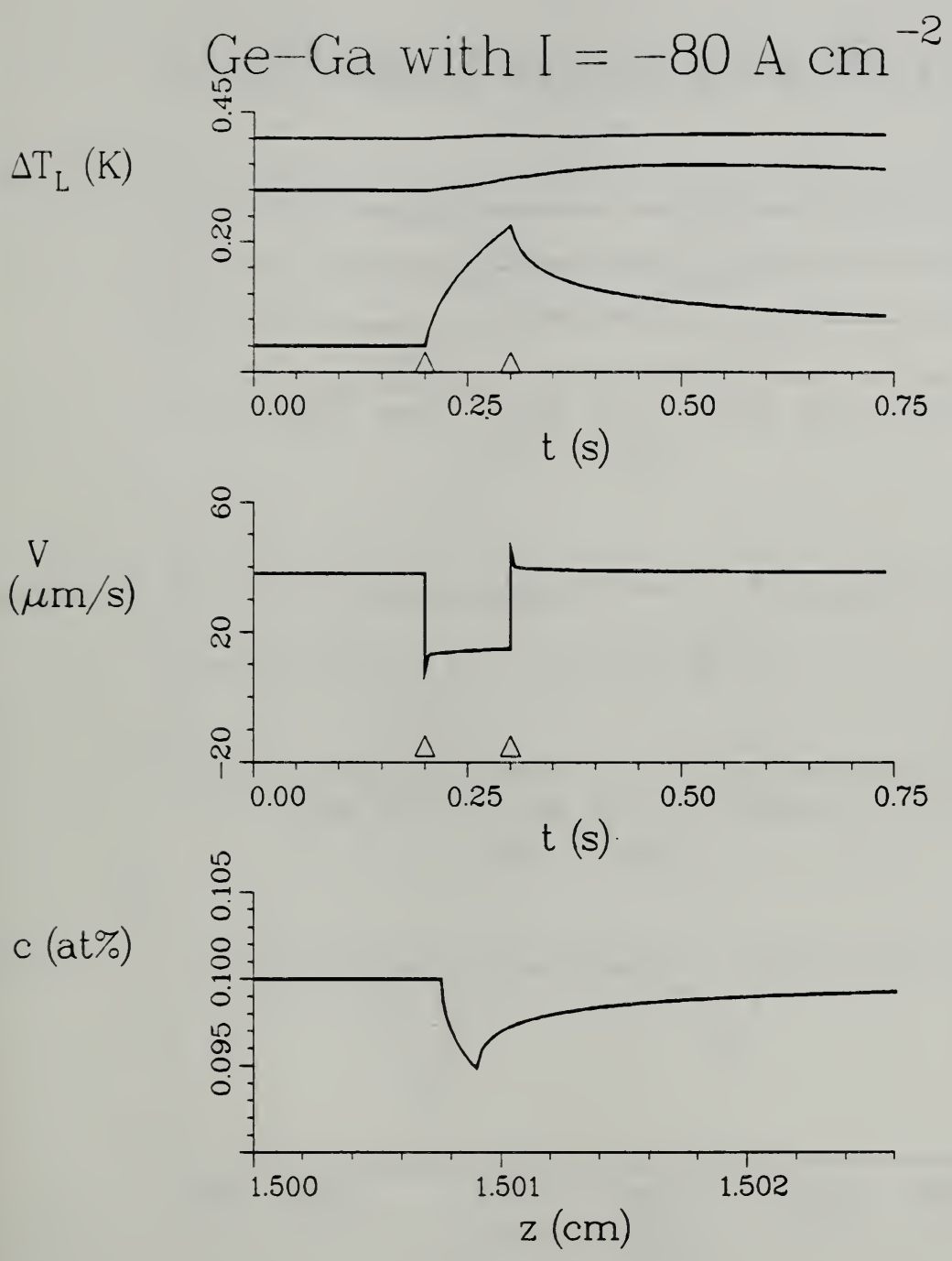
Ge–Ga with I = −80 A cm^{-2}
ΔT_L (K)
0.45
0.20
0.00
0.25
0.50
0.75
t (s)
V
(μm/s)
60
20
−20
0.00
0.25
0.50
0.75
t (s)
c (at%)
0.095 0.100 0.105
1.500
1.501
1.502
z (cm)

Figure 13

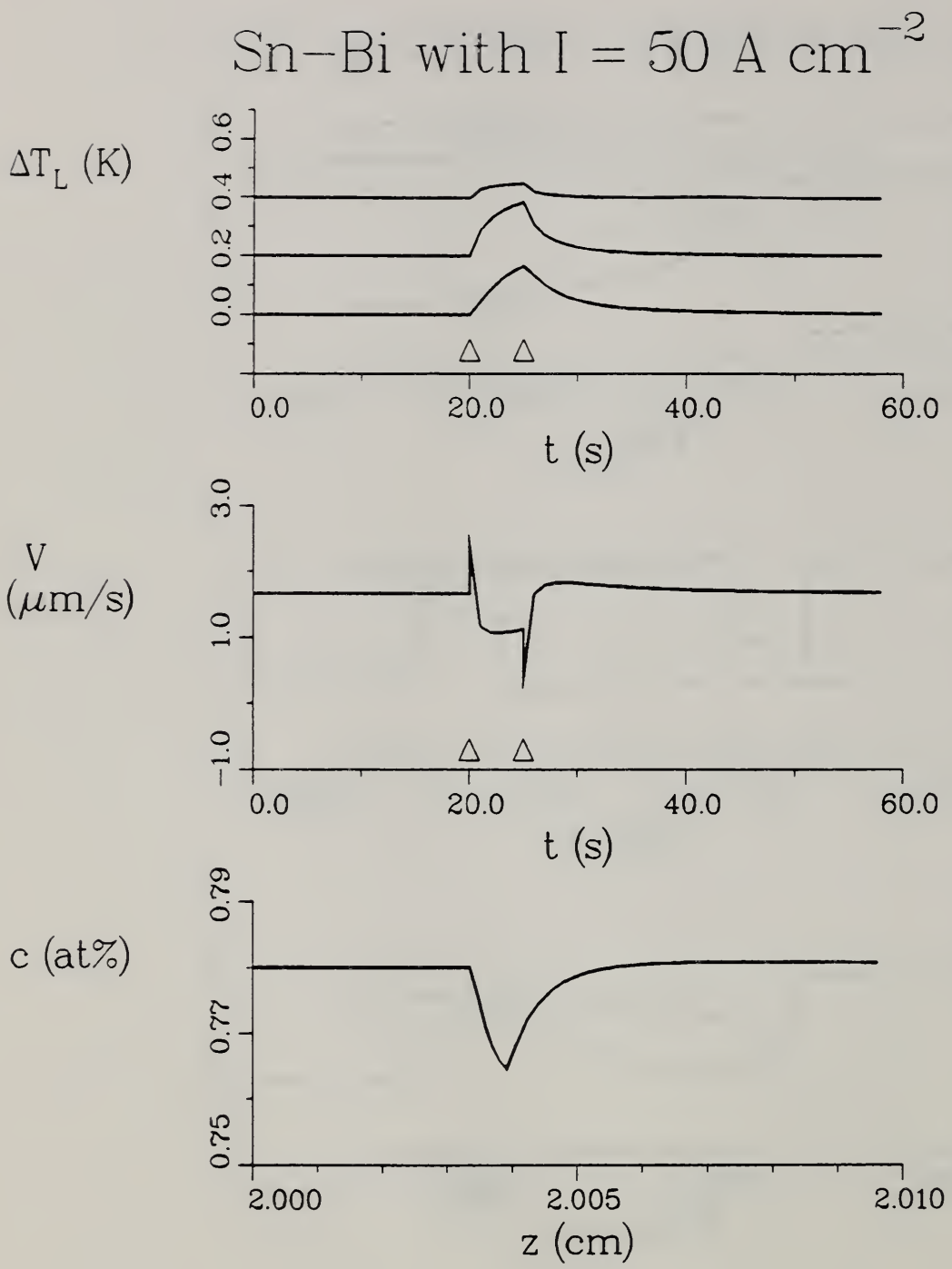
Sn–Bi with I = 50 A cm^{-2}
ΔT_L (K)
0.0
0.2
0.4
0.6
0.0
20.0
40.0
60.0
t (s)
V
(μm/s)
3.0
1.0
−1.0
0.0
20.0
40.0
60.0
t (s)
c (at%)
0.79
0.77
0.75
2.000
2.005
2.010
z (cm)

Figure 14

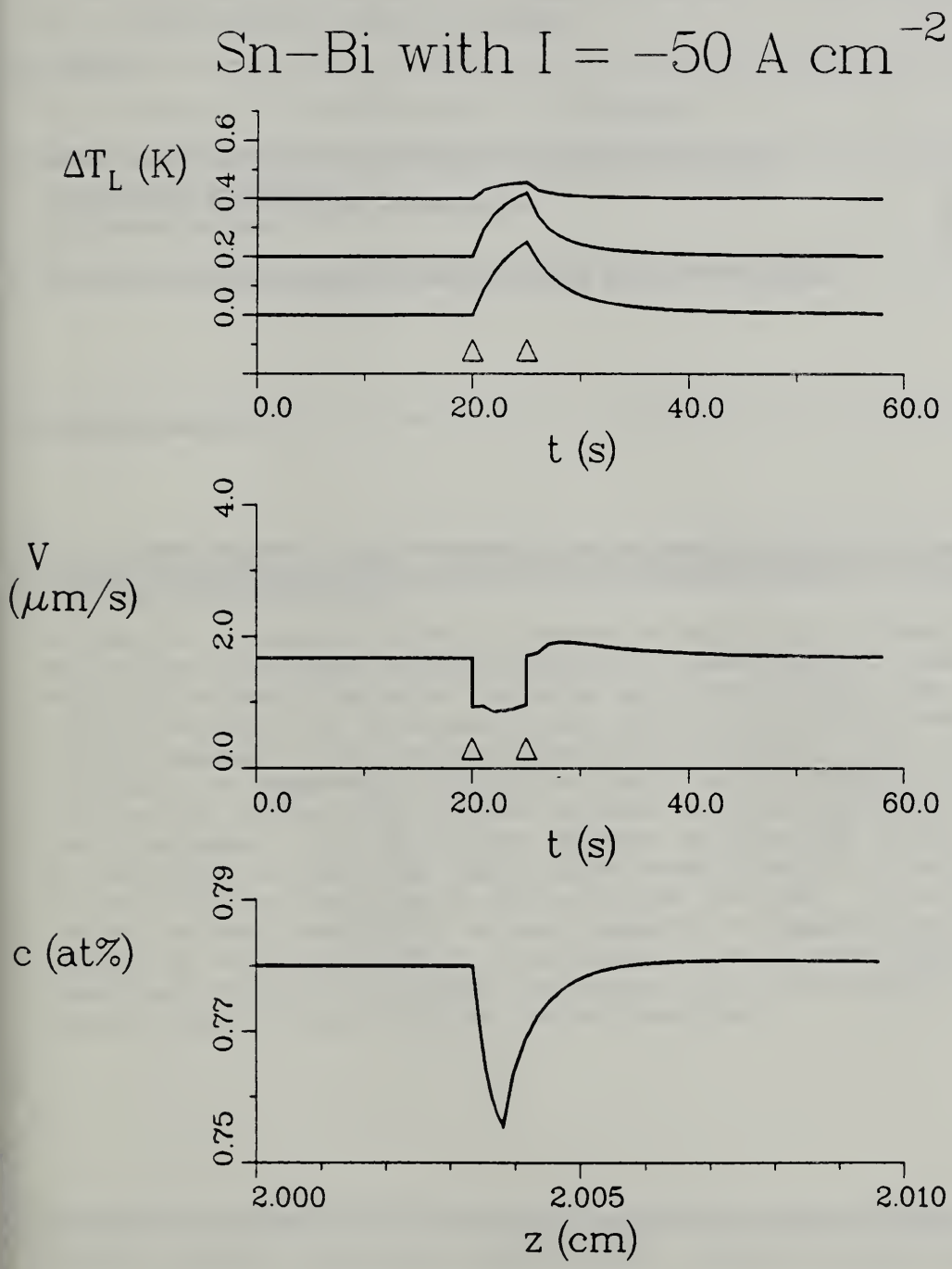
Sn–Bi with I = –50 A cm^{-2}
ΔT_L (K)
0.0
0.2
0.4
0.6
0.0
20.0
40.0
60.0
t (s)
V
(μm/s)
0.0
2.0
4.0
0.0
20.0
40.0
60.0
t (s)
c (at%)
0.75
0.77
0.79
2.000
2.005
2.010
z (cm)

Figure 15

NIST-114A
(REV. 3-89)

U.S. DEPARTMENT OF COMMERCE
NATIONAL INSTITUTE OF STANDARDS AND TECHNOLOGY

BIBLIOGRAPHIC DATA SHEET

1. PUBLICATION OR REPORT NUMBER
NISTIR 89-4161

2. PERFORMING ORGANIZATION REPORT NUMBER

3. PUBLICATION DATE
SEPTEMBER 1989

4. TITLE AND SUBTITLE

Directional Solidification of a Planar Interface in the Presence of a Time-Dependent Electric Current

5. AUTHOR(S)

L. N. Brush, S. R. Coriell and G. B. McFadden

6. PERFORMING ORGANIZATION (IF JOINT OR OTHER THAN NIST, SEE INSTRUCTIONS)

U.S. DEPARTMENT OF COMMERCE
NATIONAL INSTITUTE OF STANDARDS AND TECHNOLOGY
GAITHERSBURG, MD 20899

7. CONTRACT/GRANT NUMBER

8. TYPE OF REPORT AND PERIOD COVERED

9. SPONSORING ORGANIZATION NAME AND COMPLETE ADDRESS (STREET, CITY, STATE, ZIP)

10. SUPPLEMENTARY NOTES

[ ] DOCUMENT DESCRIBES A COMPUTER PROGRAM; SF-185, FIPS SOFTWARE SUMMARY, IS ATTACHED.

11. ABSTRACT (A 200-WORD OR LESS FACTUAL SUMMARY OF MOST SIGNIFICANT INFORMATION. IF DOCUMENT INCLUDES A SIGNIFICANT BIBLIOGRAPHY OR LITERATURE SURVEY, MENTION IT HERE.)

We develop a numerical method to study the motion of a planar crystal-melt interface during the directional solidification of a binary alloy in the presence of a time-dependent electric current. The model includes the Thomson effect, the Peltier effect, Joule heating and electromigration of solute in the coupled set of equations governing heat flow in the crystal and melt, and solute diffusion in the melt. For a variety of time dependent currents, the temperature fields and the interface velocity are calculated as functions of time for indium antimonide and bismuth, and for the binary alloys, germanium-gallium and tin-bismuth. For the alloys, we also calculate the solid composition of a function of position, and thus make quantitative predicitons of the effect of an electrical pulse on the solute distribution in the solidfied material. In addition, for a sinusoidal current of small amplitude, we have compared the numerical solutions with approximate analytical solutions valid to first order in the current amplitude. By using this numerical approach the specific mechanisms which play dominant roles in interface demarcation by current pulsing can be identified.

12. KEY WORDS (6 TO 12 ENTRIES; ALPHABETICAL ORDER; CAPITALIZE ONLY PROPER NAMES; AND SEPARATE KEY WORDS BY SEMICOLONS)

crystal growth, directional solidification, electric current, numerical solution, Peltier effect, Thomson effect, Joule heating, electromigration, interface demarcation, time-dependent

13. AVAILABILITY

[X] UNLIMITED

[ ] FOR OFFICIAL DISTRIBUTION. DO NOT RELEASE TO NATIONAL TECHNICAL INFORMATION SERVICE (NTIS).

[ ] ORDER FROM SUPERINTENDENT OF DOCUMENTS, U.S. GOVERNMENT PRINTING OFFICE, WASHINGTON, DC 20402.

[X] ORDER FROM NATIONAL TECHNICAL INFORMATION SERVICE (NTIS), SPRINGFIELD, VA 22161.

14. NUMBER OF PRINTED PAGES
52

15. PRICE
A04

ELECTRONIC FORM